geographical analysis

Geographical Analysis (2020) **0**, 1–35

How to Measure Distance on a Digital Terrain Surface and Why it Matters in Geographical Analysis

Yi Qiang[1], Barbara P. Buttenfield[2], Maxwell B. Joseph[3]

[1]Department of Geography and Environment, University of Hawaii at Manoa, Honolulu, HI USA, [2]Department of Geography, University of Colorado at Boulder, Boulder, CO USA, [3]Earth Lab, University of Colorado at Boulder, Boulder, CO USA

Distance is the most fundamental metric in spatial analysis and modeling. Planar distance and geodesic distance are the common distance measurements in current geographic information systems and geospatial analytic tools. However, there is little understanding about how to measure distance in a digital terrain surface and the uncertainty of the measurement. To fill this gap, this study applies a Monte-Carlo simulation to evaluate seven surface-adjustment methods for distance measurement in digital terrain model. Using parallel computing techniques and a memory optimization method, the processing time for the distances calculation of 6,000 simulated transects has been reduced to a manageable level. The accuracy and computational efficiency of the surface-adjustment methods were systematically compared in six study areas with various terrain types and in digital elevation models in different resolutions. Major findings of this study indicate a trade-off between measurement accuracy and computational efficiency: calculations at finer resolution DEMs improve measurement accuracy but increase processing times. Among the methods compared, the weighted average demonstrates highest accuracy and second fastest processing time. Additionally, the choice of surface adjustment method has a greater impact on the accuracy of distance measurements in rougher terrain.

Introduction

Distance is a fundamental spatial metric, which is used to measure route length, travel distance, feature size and shape, and is also the foundation of higher-order spatial metrics such as area and volume. Distance metrics provide a foundation for spatial analysis and modeling, such as buffering, pattern analysis, spatial clustering, shortest path analysis, and geostatistical analysis. The accuracy of distance measurement is of critical importance to many physical models, such as flood inundation (Tucker and Hancock 2010), avalanche risk evaluation (Gutiérrez 2012), stream extraction (Stanislawski, Falgout, and Buttenfield 2015), regional power line routing

Correspondence: Yi Qiang, Department of Geography and Environment, University of Hawaii at Manoa, Saunders 416, 2424 Maile Way, Honolulu, HI-96822, USA
e-mail: yiqiang@hawaii.edu

Submitted: 12 August, 2019; Revised version accepted: 10 July, 2020

doi: 10.1111/gean.12255

(Kiessling et al. 2014), and analysis of surface pollutants such as nitrogen (Harms, Wentz, and Grimm 2009), all of which are commonly implemented in raster data models, in order to register with terrain or imagery layers. Currently, planar distance and geodesic distance are the common surface distance metrics in geographic information systems (GIS) and geospatial analytic tools. The former metric assumes the earth surface is a flat plane and distance is the length of the straight line from Location A to B. The latter takes into account the curvature of the Earth and is used more often in longer distance measurements such as flight and shipping routes. However, neither of the two takes into account undulations and irregularities in topography, which causes uncertainty in distance measurement on a terrain surface. In this article, we refer to distance that accounts for terrain irregularity as *surface-adjusted* distance. Knowing how to accurately measure surface-adjusted distance is of critical importance for spatial models that are sensitive to distance measurement.

Theoretically, measuring distance on Light Detection and Ranging (LiDAR) data should generate the most precise measurement, relative to coarser resolution terrain. However, the availability of LiDAR data is far from comprehensive in developed nations, not to mention in rural and undeveloped regions. Additionally, storing, rendering, and processing large LiDAR point clouds can be computationally expensive, which may not be applicable or necessary in national, continental, or global modeling tasks or in applications for which coarser resolution data are sufficient. Instead, measurement on coarser resolution digital elevation models (DEMs), which are formed by a regular spatial grid of elevation values, provides a more practical solution for many analytical and modeling tasks. An alternative data model forms a network of triangular facets (Triangulated Irregular Networks or TINs) that require more computation to generate but that characterize elevations at finer resolution where terrain is more rough or uneven. DEMs are used more commonly in modeling tasks because they are faster to generate, to process, and to integrate with other data layers.

Distance measurements on DEMs rely upon two assumptions adopted historically for pragmatic reasons relating to slower computational speeds and restricted data volumes. One assumption is that the measured distance between points can be approximated by the distance between centroids of pixels containing such points. Another assumption is that pixels are flat and rigid, analogous to ceramic tiles. Reliance upon these assumptions generates inaccurate and imprecise distance measures and we will demonstrate that these inaccuracies vary notably with changing pixel size. In fact, as pixel size increases it is less likely that a point lying within that pixel sits squarely on the centroid. Moreover, terrain can bend, twist, and undulate within each pixel. With wide availability of faster computational speeds and High Performance Computing (HPC), this article argues that the two assumptions can and should be relaxed, by accepting that observed points do not commonly fall directly on a pixel centroid, and by accounting for slope and non-uniform terrain for any distance measured on a DEM.

The process of *surface adjustment* relaxes the two assumptions. To understand the distinction between distance measured on rigid pixels as opposed to surface-adjusted pixels, readers might consider the comparative analogy between measuring distance "as the crow flies" and "as the horse runs" (Buttenfield et al. 2016). The important questions to ask are first, how much improvement in accuracy can be expected at a given spatial resolution (i.e., pixel size), and second, what balance is achieved between the improved accuracy and additional computational cost required for surface adjustment. These questions form the basis for the experiments reported in this article. Answers to these questions establish a foundation for migrating GIS and spatial

analysis tools from the simplistic "as the crow flies" paradigm to the more realistic "as the horse runs" paradigm.

The analysis will gain novel insights to the effect of scale, which are commonly acknowledged in geographical analysis (Qiang et al. 2018; Qiang and Van de Weghe 2019). The experiment attempts to answer higher level questions, such as (1) do finer resolution data always provide more accurate distance measurement? (2) is there an operational scale where a geographical phenomenon (e.g., a terrain surface in this case) can be modeled most accurately? The impact of scale in terrain modeling have been reported in other studies. For instance, Usery et al. (2004) assessed deviations in DEM elevations at varying resolutions, and found that elevation values match well ($R^2 = 0.9$) for DEM resolutions between 3 m and 30 m, but gradually deviate as pixel sizes increase. Chang and Tsai (1991) evaluated the effect of DEM resolution on slope and aspect estimation and found these two indices vary with resolution and landscape changes. Kienzle (2004) conducted a comprehensive assessment of the effect of DEM resolution on a wider range of terrain indices including elevation, slope, aspect, curvature, and wetness index, and showed an increasing root-mean-square error (RMSE) of these indices as the resolution coarsens. Zhang and Montgomery (1994) assessed several topographic indices and found that 10 m grid size provides a substantial improvement over 30 m and 90 m data, but 2 m or 4 m data provide only marginal additional improvement. Moreover, varying resolution can also influence the output of seismic models based on terrain analysis (Shafique et al. 2011). All these studies demonstrate the importance of scale (or resolution) for spatial modeling in digital terrain models. This article looks into the most basic spatial metric (i.e., distance), which lays a foundation to develop scale-sensitive spatial analysis tools for terrain modeling.

Notwithstanding advances in data processing mentioned above, distance measurement on digital terrain models has not been systematically assessed, following logic that accuracy improvements are so small that surface adjustment is unwarranted. For individual pixels, inaccuracies may be small, but additive effects can propagate dramatically, especially in regional models (e.g., disaster evacuation) or global models (e.g., sea level rise). It is also uncertain how inaccuracies propagate at different resolutions and in different types of terrain (e.g., smooth or rugged, homogenous or heterogeneous). Estimating the within-pixel position of points and associated elevations can be accomplished using a variety of interpolation methods, and these may contribute also to varying degrees of inaccuracy (Ghandehari 2019). As large-scale physical models become increasingly common, especially for modeling regional and global environmental systems, compelling reasons emerge to develop surface-adjusted spatial metrics and understand the uncertainties of their accuracies in different conditions.

Buttenfield et al. (2016) conducted a pilot study to assess errors in distance measurement on six different DEMs at different resolutions. The results show that the errors generally increase at coarser resolutions, and results vary with different surface adjustment methods and in different landscapes (flat or hilly, rough or smooth). Due to the computational cost of measuring distance on different DEMs and differing terrain conditions, that pilot study was limited to the measurement of only five transects in each landscape. This study extends that pilot study by using a Monte Carlo simulation to systematically evaluate a larger sample of 1,000 transects per study area to quantify the effects of multiple variables (resolution, surface adjustment method, and terrain type) on distance measurement. The computational challenge of this simulation is overcome by parallelizing the program into multiple computing units, which reduces the total processing time to an acceptable range.

Data and study area

According to data availability and landscape diversity, six study areas are selected for this study, which are located in Louisiana (LA), Colorado (CO), North Carolina (NC), Nebraska (NE), Texas (TX), and Washington (WA), respectively. Each study area is covered by a 3 m LiDAR DEM that will be used for the benchmark measurement, and DEMs at 10 m, 30 m, 100 m, and 1,000 m resolutions, which will be used for the analytic evaluation. DEM areas range from 2,491.16 km^2 in Colorado to 7,784.93 km^2 in North Carolina.

These study areas have diverse landscapes (see Fig. 1 and Table 1). The CO study area is slim, extending from north to south along the Arkansas River Valley with mountains to the east and west, and a valley in the middle. The WA study area covers the mountainous Skagit River valley and the flatter Skagit River delta which is relatively flat. The study area in LA is flat in general, with an elevation range from –0.6 m to 68.8 m. The area west of Mississippi River Channel is very flat, while the terrain east of the river is slightly hilly with small rivers or creeks flowing from north to south. The TX study area is flat, located between Waco and Austin. The NC study area extends from the eastern part of Appalachian Mountains to the Piedmont Plateau with an elevation range from 192.59 m to 1,616.97 m. The NE study area has a homogeneous and hilly pattern, carved by numerous streams, and small drainage channels.

The 3 m LiDAR DEMs were from the USGS National Elevation Dataset (NED) and were downloaded through The National Map (https://viewer.nationalmap.gov/basic/) in 2016. By 2018, the NED DEMs were renamed 3DEP (3-Dimensional Elevation Program) seamless bare earth DEMs (Stoker, personal communication 2018). The USGS NED has seamless raster elevation data for the conterminous United States, Alaska, Hawaii, U.S. island territories, Mexico, and Canada. The accuracy of NED varies spatially due to the diversity of data sources. The overall absolute vertical accuracy of this dataset has an RMSE of 1.55 m based on the geodetic control points of the National Geodetic Survey (NGS) that have millimeter- to centimeter-level accuracies (Gesch, Oimoen, and Evans 2014). This RMSE is equivalent to 3.04 m as assessed using the National Standard for Spatial Data Accuracy (NSSDA) at a 95% confidence level.

The 10 m, 30 m DEMs were downloaded from the Geospatial Data Gateway (https://gdg.sc.egov.usda.gov/). The source for the 100 m and 1,000 m DEMs was Shuttle Radar Topography Mission (SRTM) (http://dds.cr.usgs.gov/srtm/version2_1/). The absolute vertical accuracy of this dataset has an RMSE of 4.01 m (Gesch, Oimoen, and Evans 2014). The spatial reference systems of LA, CO, NC, NE, TX and WA are NAD1983 UTM Zone 13N, 15N, 17N, 14N, 14N, and 10N, respectively. Data for all sources are independently compiled DEMs generated according to the methodology outlined in (Gesch 2007). It should be noted that the actual DEM resolutions are 1/9, 1/3, 1, 3, and 30 arc-seconds with pixel sizes that are approximately 3 m, 10 m, 30 m, 100 m, and 1,000 m, respectively. Source data for the DEM tiles are listed explicitly in the Appendix.

Methods

One thousand random transects were created in each study area, to a Monte Carlo approximation of all possible linear paths across each terrain surface. The surface-adjusted lengths of these transects were estimated using different methods, and applied to the six study areas in DEMs at four different resolutions of DEMs. Surface-adjusted transect length measurements were compared with the benchmark distances measured on 3 m LiDAR DEMs using the closest centroid

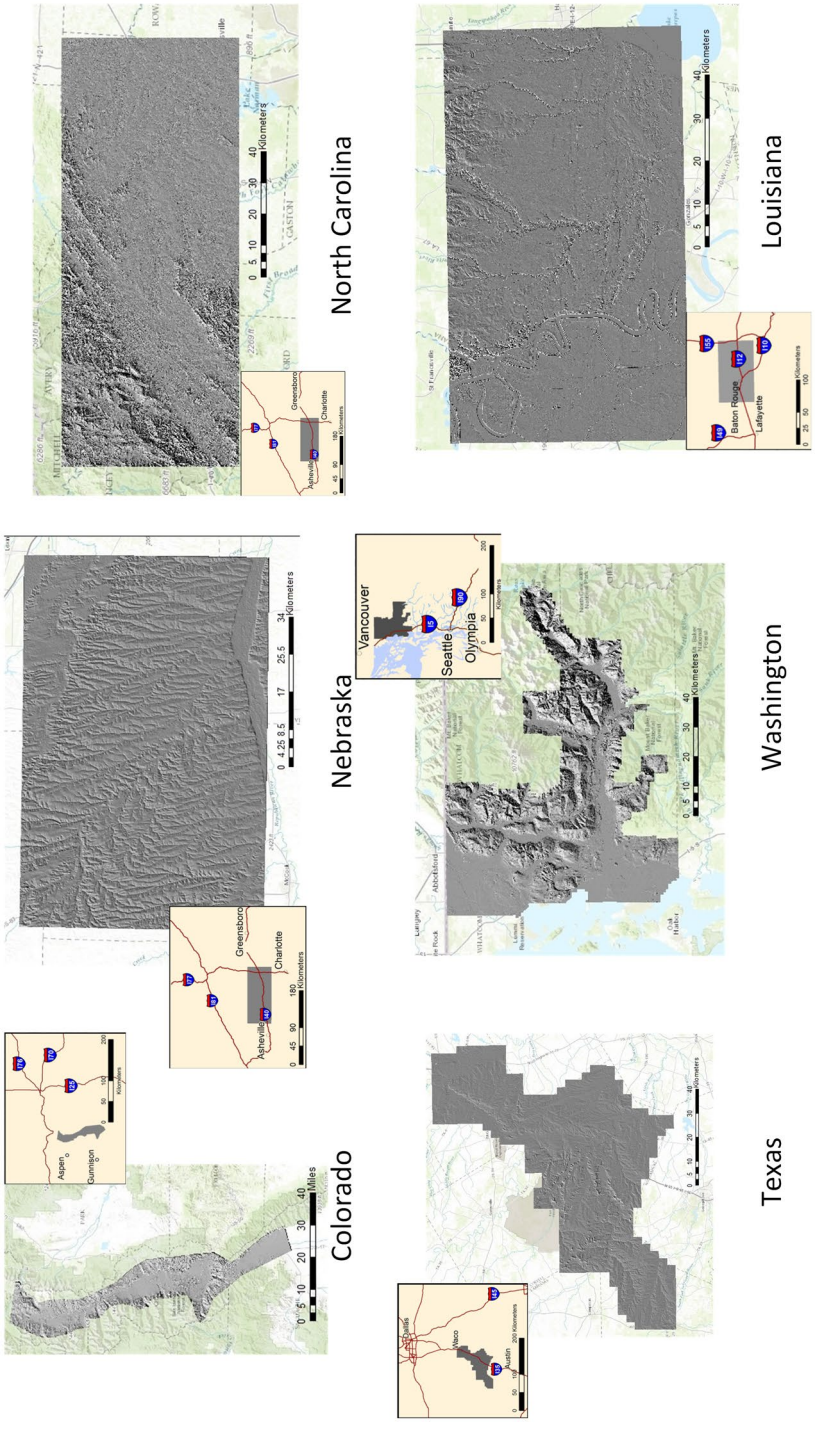

Figure 1. Study areas (figures modified from Buttenfield et al., 2016).

Table 1. Information for the Study Areas, Ranked on the Magnitude of Elevation Range

Study area	Area	Elevation range	Landscape type	DEM (10 m) size
Washington	4,530.49 km^2	–0.7 to 2,341.2 m	Mountainous	424 MB
Colorado	2,491.16 km^2	2,108.4–4,225.9 m	Mountainous	518 MB
North Carolina	7,784.93 km^2	192.59–1,616.9 m	Hilly	348 MB
Nebraska	4,708.43 km^2	635.5–937.5 m	Hilly	226 MB
Texas	5,472.56 km^2	100.0–468.8 m	Flat	667 MB
Louisiana	5,305.68 km^2	–4.6 to 70.0 m	Flat	243 MB

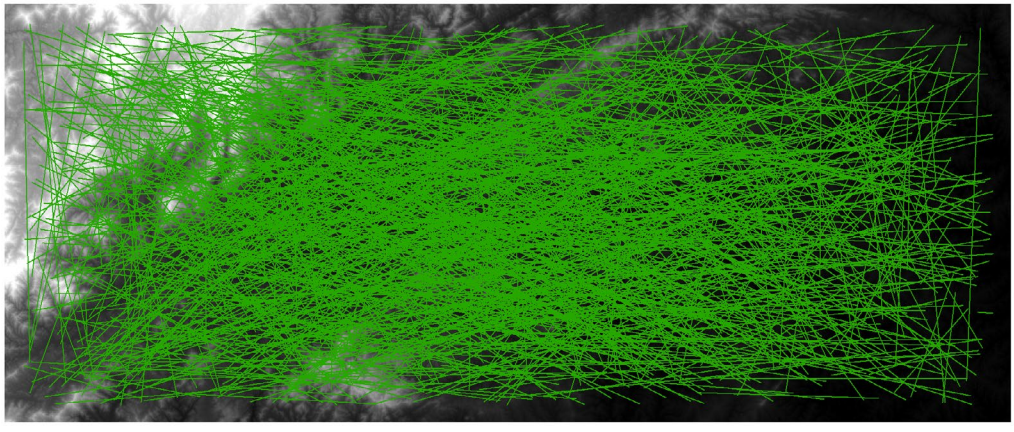

Figure 2. 1,000 transects created randomly in the study area of North Carolina.

method. The deviation of the surface-adjusted distances from the benchmark distances in different conditions was systematically evaluated, to quantify and compare accuracies of a suite of surface-adjusted distance measurement methods. The methodology of this study is described in more detail in the following sections.

Transect generation

A thousand random transects were created in each study area (e.g., Fig. 2). The transect lengths were confined to range between 900 m (30 times of the cell size of the 3 m DEM) and the longer edge of the bounding box of the study area (e.g., 84,275 m for North Carolina). Confining lengths of transects into the same range will allow comparisons of results among the study areas. As some study areas have an irregular boundary, the 1,000 transects were created in an iterative way. First, 1,000 pairs of random points were created within the DEM boundary, and linked to form 1,000 transects. Transects intersecting the DEM boundary or outside the length range were deleted. The process was repeated, generating another 1,000 transects in the same way and deleting any transects intersecting the boundary or out of the length range. The algorithm terminated when the set of valid transects contained 1,000 or more paths, from which 1,000 transects were randomly selected for the simulation. The same process was repeated, creating 1,000 transects for each of the six study areas, resulting in 6,000 transects in total. These transects are stored as comma-delimited values (csv) files recording only the coordinates of their start and end points.

Surface-adjusted measurements

Seven surface-adjusted methods are evaluated in this study. Five methods are based the DEM model and two are applied to the TIN model (Fig. 3). All surface adjustments are based upon a sampling approach. A certain number of points are randomly sampled along each transect. The number of points is dependent on the length of transect and resolution of the DEM. The point generation process is specifically detailed in Sections "Surface-adjusted measurements" and "Simulation" below. Elevations at the points are estimated using one of the seven methods described below. Distances are then computed by summing transect segment lengths between adjacent pairs of sampled points. The tested methods all incorporate elevation and slope, and differ in estimation method and in contextual information about surrounding pixels or facets, to gain a suite of surface-adjusted distance metrics. The seven tested methods are described as follows:

Methods for DEM

Closest Centroid (clos): This method is based on a sampling approach. A number of random points are sampled along the transect. The elevation of each point is taken to be the elevation of the centroid of the pixel in which the sample point is located. The overall length of a transect is the aggregation of distances between each pair of adjacent sample points. The **clos** method is used to calculate the benchmark distance in the 3 m LiDAR DEMs.

Weighted Average (wavg): This method follows the same sampling approach as for **clos**. However, the elevation of a sample point is estimated as the weighted average of the eight surrounding DEM pixels. The total length of a transect is the aggregated distance between adjacent sample points.

Polynomial Methods (3): Three polynomial methods estimate the elevations of sample points by fitting local polynomials within a specific neighborhood. The **Bilinear** method **(biLin)** fits a first order polynomial using the four pixels nearest to the sample point. The **Biquadratic** method **(biQua)** fits a second order equation to eight nearest pixels. The **Bicubic** method **(biCub)** fits a third order polynomial using sixteen nearest pixels.

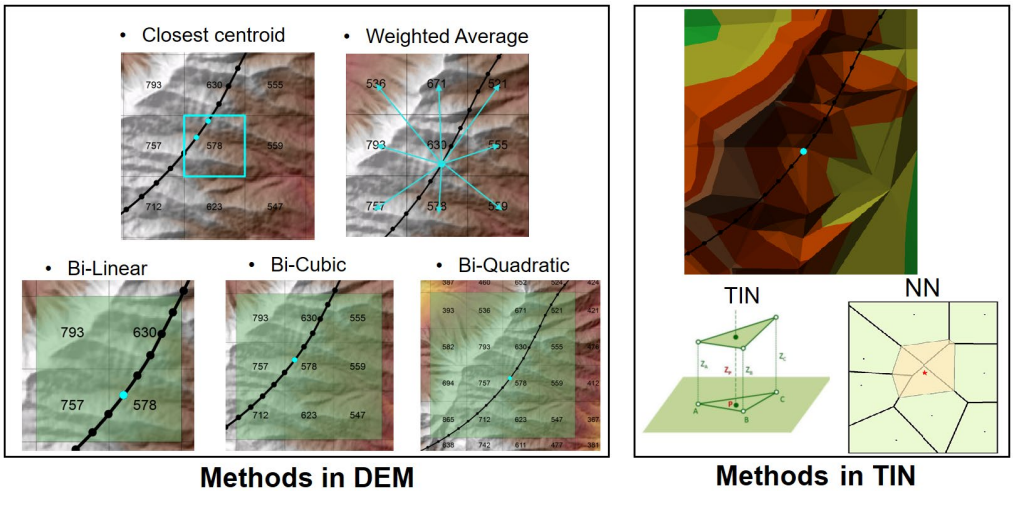

Figure 3. Surface adjustment methods and neighborhoods in DEM and TIN data models.

Methods for TIN

TIN (TIN): This method first converts the DEM into a TIN and then, interpolates the elevation of each sample point linearly from the three vertices of the triangular facet that contains it.

Natural Neighbor (NN): This method (Sibson 1981) first converts the TIN centroids into Thiessen polygons. Then, the (off-centroid) sample points seed a second layer of Thiessen polygons. The proportion of overlap between the two layers weights interpolation of the elevations of the sample points.

Simulation

The distances along the 1,000 transects in six study areas were measured using the seven surface adjustment methods and at four different resolutions. The derived surface-adjusted distances were then compared with benchmark distances measured on 3 m LiDAR DEMs to evaluate accuracy. For each transect, the distance measurement used the seven surface adjustment methods and DEMs at four resolutions (10 m, 30 m, 100 m, and 1,000 m). Distance was measured by selecting points randomly along each transect, and summing the lengths between adjacent point pairs. For the LiDAR benchmark, distances were measured using the **clos** method as described above, thus summing distances between adjacent pixel centroids to give (on average) 3 m resolution. Point sampling was thinned to preserve proportional sampling for the four test resolutions, and to avoid oversampling. To give a sense of the data volume involved in the simulation, consider a perfectly situated east-west transect with a length of 90 km. It would cover 30,000 pixels at LiDAR resolution, and have 30,000 points sampled randomly along its length for the simulation. Thinning to 10 m resolution would reduce the sampling rate to select 9,000 points randomly. Likewise, a random sample of 3,000 points would be collected at 30 m; and 900 points at 100 m, and 90 points at 1,000 m resolution.

Using sequential programming, the simulation could be implemented as a nested "for loop," which calculated the distance for 1,000 random transects per study area, in DEMs at 4 resolutions, using 7 methods and in 6 study areas. The estimated processing time for the entire simulation would exceed 500 h (~21 days). The following pseudocode shows the sequential workflow; and the number in the parentheses are the number of elements in each loop:

```
for study_area in list_study_area (6):
  for DEM in list_DEM (4):
      for method in list_method (7):
          for transect in list_Transect (study_area, 1000):
            DistCalc
```

Since distance calculations of the transects are independent, the simulation can be partitioned into parallel tasks for simultaneous processing in multiple computing units. Each computing unit calculates the distance of a transect using a specific surface adjustment method, on a single DEM at a single resolution. By doing so, the simulation can be partitioned into 168,000 (1,000 transects × 4 DEMs × 7 methods × 6 study areas) independent processes, which can theoretically complete the simulation in ~10.7 s if all processes are run concurrently. As will be discussed in the results section, average processing times ranged between roughly 5 s and more than 80 s for these DEMs at 10 m resolution, depending on transect lengths.

The simulation program is developed in Python, using open-source spatial analysis packages including numpy (Oliphant 2006), GDAL (GDAL/OGR contributors 2020), and natgrid (University Corporation for Atmospheric Research (UCAR) 2004). The open-source program is transferable across platforms and can be easily implemented in supercomputer clusters. The

parallel computing uses the IPyparallel module (The IPython Development Team 2018), which is IPython's architecture for parallel and distributed computing. The IPyparallel module supports different modes of parallelism including Single Program, Multiple Data (SPMD) parallelism, Multiple Program, Multiple Data (MPMD) parallelism, and Message Passing Interface (MPI). The distance computations of transects in different conditions are compiled into a *map* function, which simultaneously applies a function to lists of inputs and returns a list of outputs. The IPyparallel module supports a parallel version of the *map* function, which can dynamically balance the workload assigned to different processor cores. The simulation program iteratively applies a distance calculation function to four lists of parameters, which are transects, study areas, DEM resolutions, and surface-adjusted methods. The simulation was conducted with 16 × 3.2 GHz processor cores and 64 GB RAM. The program can also run in Amazon Elastic Compute (EC2) Cloud cloud-based servers. The simulation program for this study is shared in a GitHub repository (https://github.com/qiang-yi/surface_adjusted_distance).

```
# Create a LoadBalancedView object that dynamically balance workload to the computing
instances
lview = rc.load_balanced_view()

# Use a map function to execute the distance calculation for each transect, method, DEM
resolution and study area.
distance = lview.map(Calculation,

                cases_df['transect'].tolist(),
                cases_df['method'].tolist(),
                cases_df['resolution'].tolist(),
                cases_df['study_area'].tolist())
```

Memory control

The location (i.e., the start and end coordinates) of the transect and the DEM raster are the inputs for surface-adjusted distance calculation in DEM (Fig. 4a). To compute the distances of 1,000 transects, the DEM raster needs to be opened 1,000 times in memory, which can quickly exceed the RAM of a computing node. For instance, if the 10 m DEM of the smallest study area is opened 1,000 times, a total amount of 503 GB memory will be occupied, which exceeds the total RAM of most computing nodes. Also, opening the entire DEM for a single transect is an unnecessary redundancy which may increase overhead when passing data across nodes. To solve this problem,

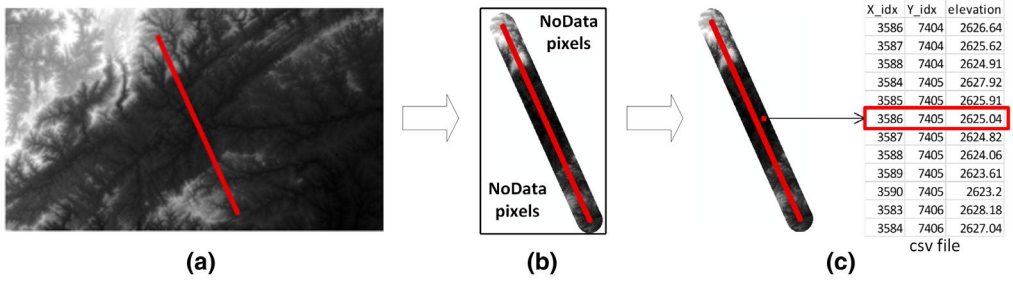

Figure 4. Converting the buffer area of a transect into a list of X-Y-Z tuples: (a) the entire DEM; (b) the DEM buffer in raster format; (c) the DEM buffer in csv format.

a buffer is built around each transect; and only the transects and buffer areas around them are sent into a distance computation. Instead of storing the buffer areas in raster, which still contain numerous no-data pixels within the Minimum Bounding Rectangle (e.g., Fig. 4b), pixels inside the buffer areas are converted into X-Y-Z tuples, which are stored in comma-separated values (csv) files (Fig. 4c). By doing so, the input data size for distance calculation of a transect can be reduced from > 100 MB to ~1 MB. The data conversion process introduces additional computational cost associated with the overhead of generating csv files for each path. However, the smaller DEM buffers increase the efficiency of distance computation by reducing computational overhead of data transfer to and from the computing nodes, and reducing overall memory requirements.

Results

Distances calculated using different surface adjustment methods on DEMs of different resolutions are compared with the benchmark distance measured at 3 m LiDAR data using the Closest Centroid method. Residuals and Root-Mean-Square Error (RMSE) metrics between the measured distances and benchmark distances evaluate the measurement accuracy. Processing times of distance measurement are also compared, to evaluate the computational efficiency of the different interpolation methods.

Residual analysis

Residuals indicate discrepancies between the measured distances and benchmark distances in the simulated transects (i.e., measured distance—benchmark distance). Fig. 5 shows that the residuals of most methods (except closest centroids) are negative at finest resolutions, indicating underestimation, but at coarser resolutions, approaching zero or becoming positive. As an exception, the closest centroid (clos) method overestimates distances at finer resolutions and transitions to underestimation as pixel size increases. Magnitude of residuals for this method is highest IN most situations except the 1,000 m resolution where the residuals of the various methods converge. The weighted average (wavg) residuals are generally closer to zero than all other methods, while the TIN and Natural Neighbor methods have the largest negative residuals. Comparing the three polynomial methods, the residuals of the bilinear method most closely approximate the benchmark (i.e., lowest absolute residuals), followed by the biquadratic, and bicubic methods. Thus, the increasing complexity of the polynomial function actually reduces accuracy of distance measurement, likely due to overfitting.

Maximum residual values are higher for more mountainous and hilly landscapes, and the magnitude of errors appears to relate as much or more to terrain roughness (i.e., elevation range, as shown in Table 1) as to DEM size: Washington is roughly the same size as Nebraska and yet, contains much larger residuals. Colorado is not even half the size of Louisiana and yet, its residuals are larger by orders of magnitude. Working across spatial resolutions, the progression of residual values generated by all methods differs most strongly at 10 m and then, resolves as pixel size increases to 1,000 m. Residuals for the three flattest terrains tend to converge at 100 m resolution, diverging by 10–20 m as overestimation becomes evident for 1,000 m pixels. This finding possibly implies that variations in accuracy of the different interpolation methods relates to terrain flatness, or perhaps to terrain uniformity. Confirmation of this would require further characterization of the DEM surfaces.

The simulated transects vary in length, and the residuals are highly dependent on the transect length. To eliminate the effect of transect length, ratios of the residuals by transect lengths were calculated to compare the measurement accuracy per distance unit. Fig. 6 shows that the

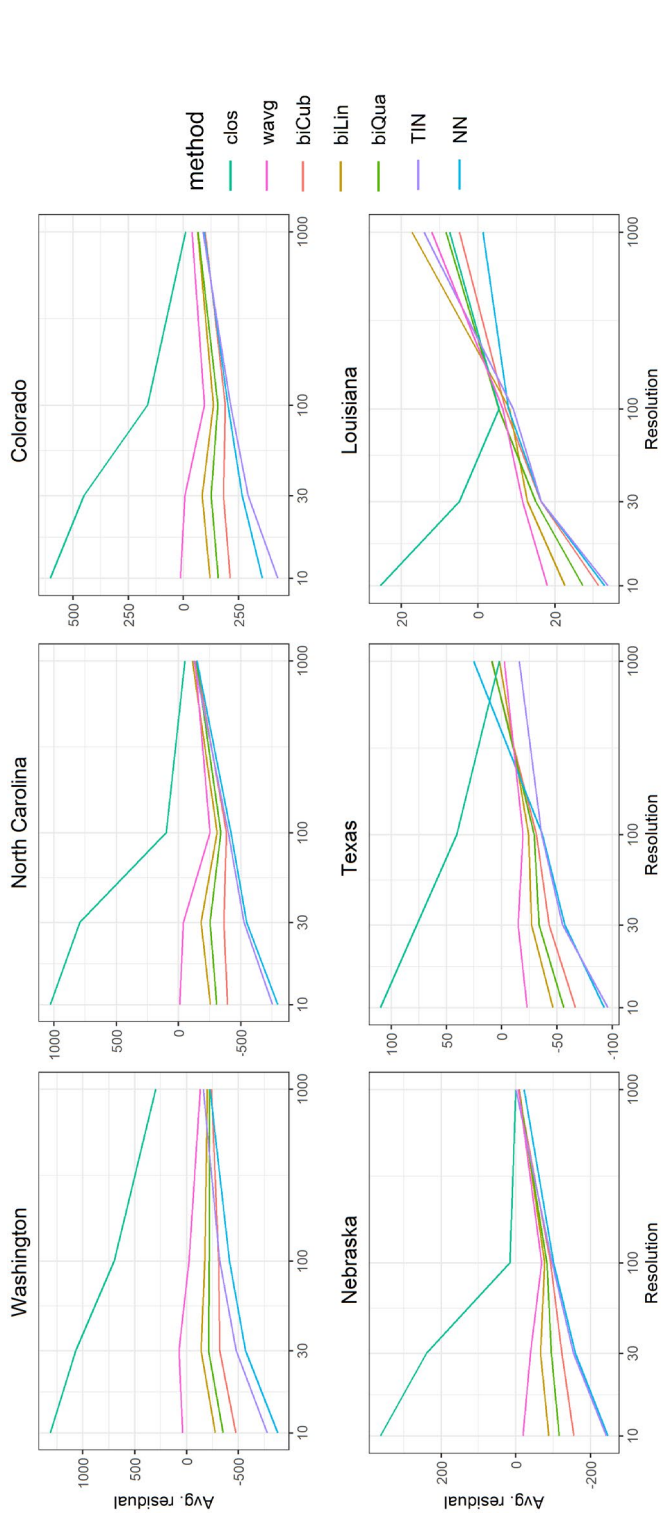

Figure 5. Mean residuals (measured in meters) between measured distances and benchmark distances at different resolutions. Positive values reflect over-estimation and negative values reflect under-estimation, relative to the LiDAR data. The *y*-axes are linear and vary among DEMs; and the *x*-axes are exponential and identical. For any particular location and resolution, methods with lines closest to zero on the *y*-axis are more accurate on average.

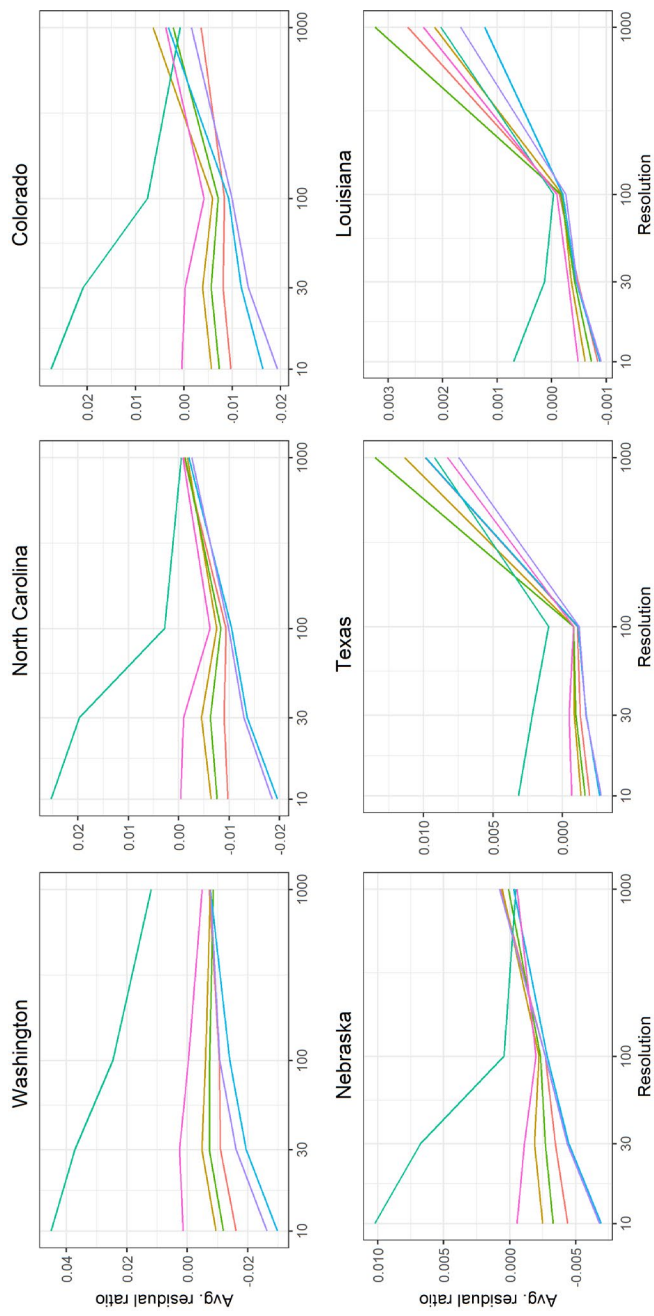

Figure 6. Mean residual ratios between benchmark distances and measured distances measured at different resolutions. Positive values reflect over-estimation and negative values reflect under-estimation, relative to the LiDAR data. Note that the *y*-axes differ across DEMs, while the *x*-axes are consistent and logarithmically rescaled.

changing pattern of the ratios of residuals at different resolutions are analogous to the patterns of residuals shown in Fig. 5. As shown in Fig. 6, the error ratio of distance measurement for any given transect may range from –2% to +4%, depending on the surface-adjusted method, the study area, and on the resolution of the DEM. Comparing among the study areas, Louisiana has the smallest error magnitude with residual ratios ranging from –0.1% to 0.3%, while the residual ratios in Colorado span ranging from –0.2% to 2.7%, indicating that distance measurement error tends to be larger in mountainous or uneven terrains than in flatter or smoother terrains.

RMSE analysis

Root-Mean-Square Error (RMSE) indicates the absolute fit between measured distances and benchmark distances. The RMSEs in Fig. 7 generally confirm the patterns of residuals in Figs. 5 and 6, with some interesting cross scale patterns highlighted. RMSE values tend to rise as pixel size increases from 100 m, with RMSE increasing for North Carolina and Colorado for 30 m and larger pixels. Method-specific errors show greatest differences at finer resolutions, resolving to a value ranging between roughly 450 m (Nebraska) and 600 m (all other study areas) at 1,000 m resolution. The range of average error among methods is higher for mountainous and hilly landscapes, with almost no difference among methods for the two flattest landscapes (Texas and Louisiana). The Weighted Average method generates the lowest RMSE magnitudes overall, although the Closest Centroid method gives lower RMSE values at 100 m resolution, for reasons that are not clear. The bilinear method has the lowest RMSE of all three polynomial methods, followed by the biquadratic and bicubic method.

Processing time

Processing time of the distance calculation increases at finer resolutions (i.e., as cell size decreases) (Fig. 8). TIN and Nearest Neighbor require the longest processing times, except for North Carolina at 10 m resolution. Shortest processing times are used by Weighted Average and Closest Centroid, followed by the bilinear polynomial. Processing times drop considerably for coarser resolution DEMs, because of relatively fewer pixels. Considering the changing patterns of residuals and RMSEs, however, there is a trade-off between accuracy and computational efficiency.

Comparing among the different methods, the Natural Neighbor and TIN method require the longest processing time in most landscapes. Given their high residuals and RMSEs, these two methods seem the least optimal for surface-adjusted distance calculation. And while the Closest Centroid method takes the shortest processing time, the accuracy metrics indicate that its utility for surface-adjusted distance estimation is highly varied, and thus, not consistently reliable. The bilinear polynomial method gives more accurate estimations but takes additional processing time, especially at fine resolutions. Given the low absolute residuals and RMSEs in most landscapes and at most resolutions, the weighted average method can be considered the surface adjusting method that best balances accuracy with processing time for distance calculation.

Discussion and implications

This study applies a HPC-enabled Monte-Carlo simulation to evaluate seven surface adjustment methods for distance calculation on digital terrain. Distances of 1,000 randomly generated transects were calculated in six study areas using different surface adjusting methods and DEMs at different resolutions. The calculated distances were compared with benchmark distances

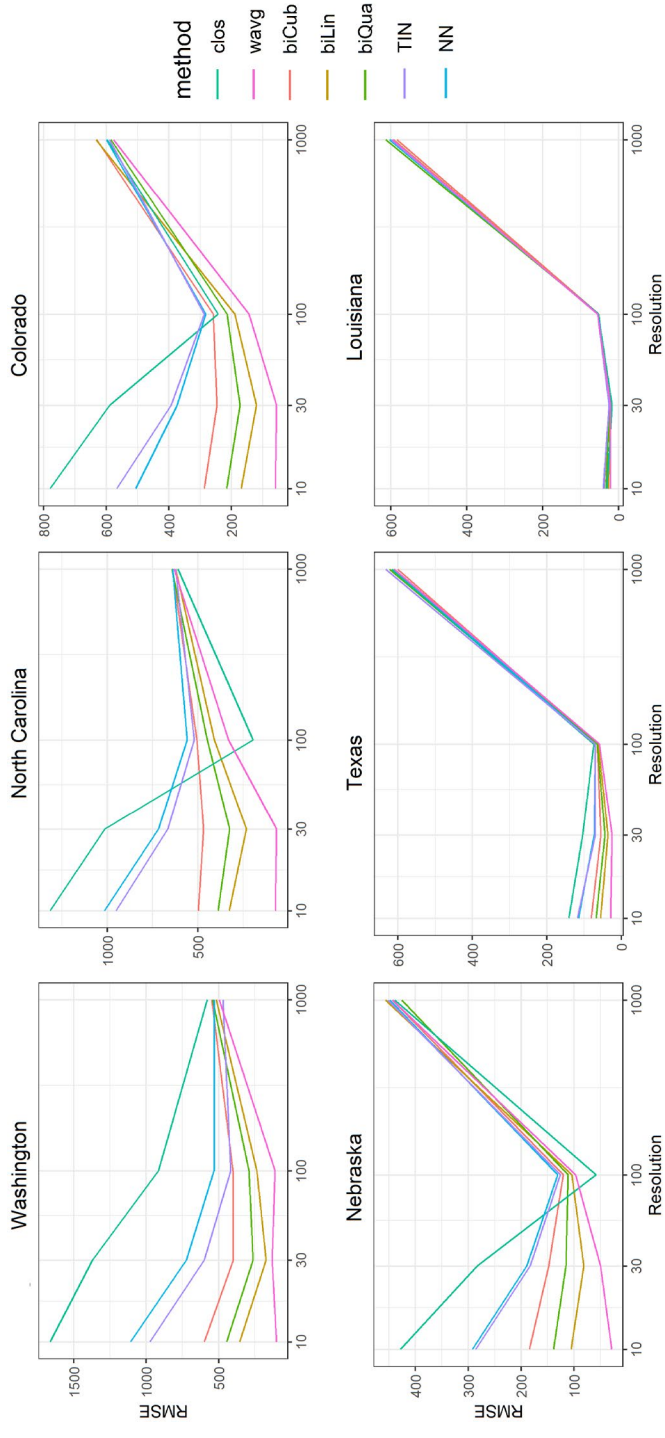

Figure 7. RMSE (measured in meters) between benchmark distances and measured distances measured in different resolutions. Note that the *y*-axes are scaled differently across panels.

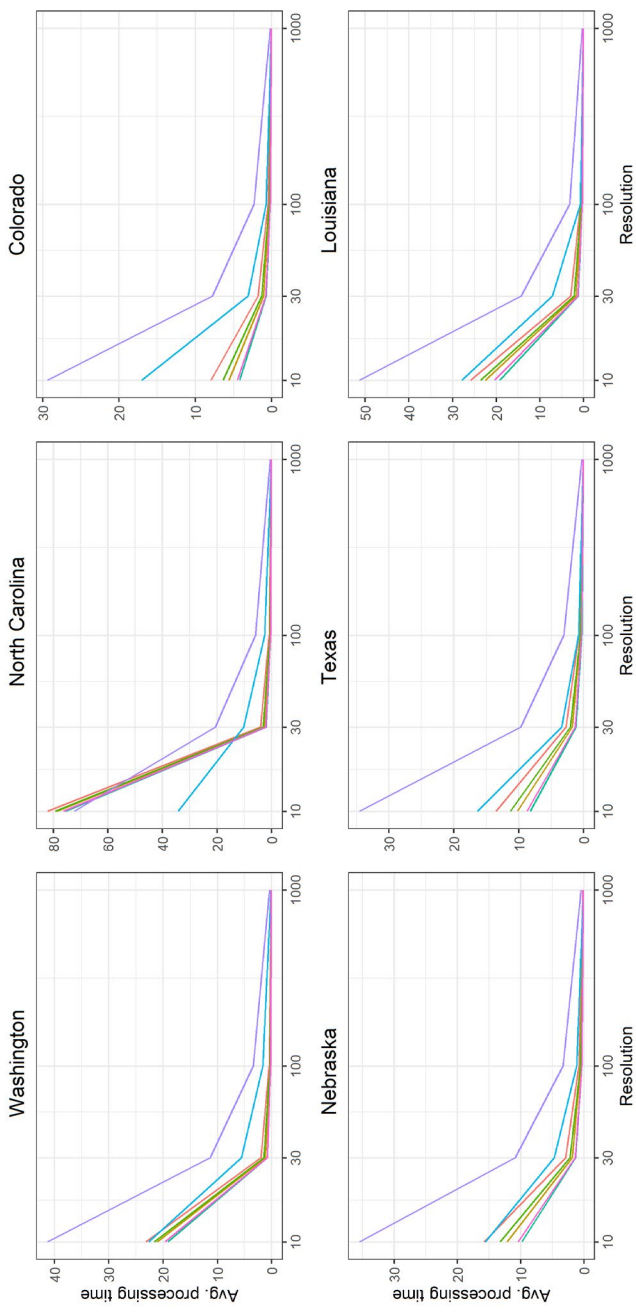

Figure 8. Mean processing times (measured in seconds) for surface-adjusted distance calculation per transect using different methods and at different resolutions. Note that *y*-axis values differ among DEMs, while *x*-axis values are identical.

measured on 3 m resolution DEMs to evaluate their accuracies. Residuals and RMSEs compared measured distances with LiDAR benchmark distances. To reduce the overall computing time, the distance calculation algorithm was optimized to reduce memory usage and processing time in a multi-core computer.

The major findings in this study include: (1) the distance measurement varies with DEM resolutions, surface adjustment methods and terrain types; (2) Weighted Average is overall the most accurate surface adjustment for distance measurement with a few exceptions; (3) there is a trade-off between DEM resolution and computing time. The assessment results provide a foundation for distance-based spatial analyses on terrain surface (e.g., distance-based point pattern analysis and kriging interpolation). In a broader sense, the study increases the understanding about the interplay between analytic methods, scale and the geographical phenomena being studied.

The assessment reveals the dependency of distance measurement on data resolution, surface adjustment methods, and terrain variations. The results show a pattern of distance underestimation relative to the LiDAR benchmarks at finer resolutions (10 m and 30 m) that transitions to near equivalence or slight overestimation as pixel size increases. The degree of underestimation varies with method of surface adjustment. The weighted average method has the highest accuracy overall in most situations. This finding may seem surprising given that the method utilizes a search neighborhood of only 8 adjacent pixels. In terrain with high local relief, one might expect that the polynomial methods would provide better results due to larger neighborhoods and/or adjustment methods that could filter localized perturbations in elevation. The results indicate that biquadratic (8 neighbors) and the bicubic (16 neighbors) methods tend to exaggerate underestimation. While the bilinear neighborhood (4 pixels) produces residuals and RMSE values closer to the weighted average, the kernel is rarely centered on the point being adjusted, and this can over- or underemphasize nearby terrain nonuniformity. Closest Centroid, TIN and Nearest Neighbor employ even smaller neighborhoods (1, 3, and up to 6 neighbors, respectively) further exacerbating the problem. Overestimation of surface-adjusted distance for all methods at 1,000 m resolution may be associated with neighborhood bias as well: the spatial extent of larger pixels may ignore local features at the same time as weighting more distant features (up to 4, 8, or 16 kilometers away) in equal consideration. The weighted average method adjustment is based on central tendency and qualified by inverse distance weighting, which can offset the impacts of rough or uneven terrain in more distant pixels.

The balance between improved accuracy and extra processing time is relevant from a practical standpoint. The DEMs tested here are probably too small to be useful for regional or continental modeling, as for example studies involving sea level rise, earthquake damage, or coastal storm events. Even with high performance computing, distance adjustment for larger study areas could require minutes or longer. Moreover, distance estimation is often the initial step, and rarely the final product of spatial modeling. The Closest Centroid method calculates distance based on elevation in rigid pixels, which does not adjust the terrain surface using surrounding elevation values. Thus, the distance measurements of this method fluctuate at different resolutions due to the stair-step effect of DEM pixels. As a consequence, the method tends to over-estimate distance at finer resolutions due to including too many (small) pixels, and to under-estimate distance at coarser resolutions due to averaging within large pixels. Despite carrying the lowest processing time, the accuracy of the Closest Centroid method should not be considered a good choice when trying to balance accuracy with processing times. Higher processing times shown by TIN and Nearest Neighbor are coupled with reduced accuracy, and no balance is achieved. Polynomial adjustment by second and third order equations reflects similar results. Given the second lowest processing time, the weighted average method can be considered the optimal surface adjusting

method for distance calculation in most situations. Adjustment using bilinear polynomial estimation can be considered an alternative, with slightly less improvement in accuracy.

The accuracy of the surface adjustment methods also varies in different terrain types. The accuracy difference among methods is smallest in flat terrain such as Louisiana and Texas, implying that for these terrain types, the choice of surface adjustment for distance measurements matters less than for hilly and mountainous terrain. Differences in error metrics for more mountainous or nonuniform terrains show greater variation especially at fine and intermediate resolutions, meaning the choice of surface adjustment appears to have a greater impact on distance estimation in rougher terrain and at finer resolutions. Error magnitudes begin to coalesce after 100 m resolution for all methods, indicating that at some point, the extra computations required for surface adjustment are simply not worth the potential improvement in accuracy. Accuracy of surface-adjusted distance measurement is reduced in DEMs that contain a mix of terrain types, with some flat and some hilly areas. Future research must investigate the relationships between terrain roughness, terrain uniformity, and accuracy to better understand the full implication of these findings.

As an additional note, methods that perform best for distance calculation may or may not be optimal for other tasks such as estimating surface-adjusted elevation or area. Ghandehari, Buttenfield, and Farmer (2019) demonstrate that linear and bilinear polynomials give slightly better accuracies for surface-adjusted estimation of point elevation on DEMs, although errors for any method are quite small, on the order of centimeter magnitudes for terrain measured in meters. Their study shows however that errors for all methods increase in rough terrain. This reflects earlier research by Shi and Tian (2006) and Schneider (2001) showing that errors in elevation estimation are more prominent in rough terrain. Ghandehari and Buttenfield (2018) compare surface-adjusted methods for estimating pixel surface areas, finding that while a bicubic polynomial estimation gives the highest accuracy, relative to a 3 m LiDAR benchmark, it carries unreasonably high processing times. They modify Jenness' (2004) surface area estimation method and then apply bilinear polynomial estimation to achieve nearly equivalent accuracies to the bicubic method, with processing times reduced by nearly 80% (Ghandehari 2019).

As the primary objective of the study is to evaluate and compare among surface adjustment methods, the simulation program is implemented in a simple parallel model, which effectively reduces the computing time to a manageable level. The performance of the simulation can be further improved with finer grain parallelism architectures such as OpenMP and MPI. Also, the program can be further parallelized by including on-the-fly transect generation and buffer area extraction. These optimization options will be explored in future experiments such as surface-adjusted area calculation for a new variety of case studies.

The title of this article raises the issue of why accurate distance measurements matters in geographical analysis. There are several reasons. First, and as described at the beginning of the article, distance metrics underlie many if not most simple and compound GIS analytic methods. Second, it stands to reason that inaccurate distances can propagate inaccuracies throughout the entire course of spatial modeling and confound any estimates related to terrain surfaces, as for example glacial recession, wetlands fragmentation, freight routing, or debris flow estimation. Third, digital terrain is one of the most frequently included data layers in spatial analyses. Bolstad (2019, p. 485) cites the influence of terrain characteristics on a broad set of environmental functions such as soil moisture, agricultural yields, sediment transport, and construction costs. Wilson (2012, p. 107) explains the important impact of terrain "… in modulating the atmospheric, geomorphic, hydrologic, and ecological processes operating on or near the Earth's surface." He refers to Hutchinson and Gallant (2000) in arguing that the terrain is so tightly coupled with these four

families of processes that characterization of the terrain directly leads to and refines insights about the nature of the processes. In a nutshell, geospatial analytics cannot be accurate without accurate distance metrics. And because most geographic and geomorphic processes depend partially or wholly upon the land surface on which they are situated, distance measurements should be performed on the terrain surface, "as the horse runs" instead of "as the crow flies."

With the emergence of parallel processing and the increased availability of fine resolution terrain data, surface-adjusted distance metrics are becoming an operational strategy that can improve the accuracy of many types of spatial modeling, although results depend upon several factors (resolution, terrain type and uniformity, and surface adjustment method). Three of those factors have been examined here, but this study has limitations that call for additional examination and assessment. The characterization of terrain uniformity must be examined more formally, along with possible interaction among the factors analyzed in this article. Additionally, the optimal methods choices need to be further tested and validated by embedding the surface-adjusted distance metrics into more complex analytics. For instance, a hypothesis to be tested is whether surface-adjusted distance can increase the accuracy of kriging interpolation. Surface adjustment also needs to be embedded in full-blown surface process models to understand them in analytic practice. And finally, the assessment of distance measurement shows that choosing an appropriate (not necessarily the finest) scale is important for spatial analysis and modeling. Quattrochi and Goodchild (1997) suggest that geographical analyses should be conducted at the operational scale (also referred to by Montello (2001) as phenomenon scale) where the studied processes operate since slight changes in these processes can invoke pronounced changes in model results. The results reported in this study reveal that the optimal DEM resolutions for distance measurement varies among different surface adjustment methods and terrain types. Importantly, the choice of a method may also depend upon task (measuring distance, surface area, or volume). As distance is the most fundamental metric for geographical analyses, the knowledge generated in this study lays a foundation for developing scale-sensitive analysis tools on a terrain surface.

Acknowledgment

The authors acknowledge excellent and constructive comments from reviewers, which strengthened the text.

Funding information

This article is based on work supported by the U.S. National Science under the Methodology, Measurement & Stats (MMS) Program (Award No. 1853866). This article is also based on work that is part of the Data Harmonization Initiative at Earth Lab (https://www.colorado.edu/earthlab/), supported by an investment from the University of Colorado Grand Challenge Initiative. Any opinions, findings, and conclusions or recommendations expressed in this material are those of the authors and do not necessarily reflect the views of the funding agencies.

Appendix

This appendix documents the data sets and their download sources used for the experiments in the manuscript. The exact specifications are included here in the interests of reproducible science, so that interested readers can replicate the study using the same data sets.

Benchmark LiDAR data

State	Benchmark LiDAR datasets
Colorado	2010 South San Luis Lakes Lidar
Nebraska	2009 Nebraska Department of Natural Resources (DNR) South Central Nebraska Lidar
North Carolina	2003 North Carolina Floodplain Mapping Program (NCFMP) Lidar
Texas	2011 Texas Natural Resources Information System (TNRIS) Lidar: Bell, Burnet, and McLennan Counties
Washington	2006 USGS Lidar: North Puget Sound, Washington
Louisiana	1999 Louisiana Lidar Project (1999–2008)

Tiles of 10 m DEMs

The following tiles are available to download in USGS TNM Download: https://viewer.nationalmap.gov/basic/

State	Tiles of 10 m DEM
Colorado	USGS NED ned19_n39x25_w106x25_co_arkansasvalley_2010 1/9 arc-second 2012 15 × 15 min IMG USGS NED ned19_n39x00_w106x50_co_arkansasvalley_2010 1/9 arc-second 2012 15 × 15 min IMG USGS NED ned19_n38x75_w106x00_co_arkansasvalley_2010 1/9 arc-second 2012 15 × 15 min IMG USGS NED ned19_n39x50_w106x00_co_grandco_2010 1/9 arc-second 2011 15 × 15 min IMG USGS NED ned19_n38x75_w106x50_co_arkansasvalley_2010 1/9 arc-second 2012 15 × 15 min IMG USGS NED ned19_n38x25_w106x25_co_sanluisvalley_2011 1/9 arc-second 2012 15 × 15 min IMG USGS NED ned19_n38x50_w106x00_co_arkansasvalley_2010 1/9 arc-second 2012 15 × 15 min IMG USGS NED ned19_n38x25_w106x00_co_arkansasvalley_2010 1/9 arc-second 2012 15 × 15 min IMG USGS NED ned19_n38x25_w106x25_co_arkansasvalley_2010 1/9 arc-second 2012 15 × 15 min IMG USGS NED ned19_n39x25_w106x50_co_arkansasvalley_2010 1/9 arc-second 2012 15 × 15 min IMG USGS NED ned19_n38x25_w106x00_co_sanluisvalley_2011 1/9 arc-second 2012 15 × 15 min IMG USGS NED ned19_n39x00_w106x00_co_arkansasvalley_2010 1/9 arc-second 2012 15 × 15 min IMG USGS NED ned19_n39x50_w106x25_co_arkansasvalley_2010 1/9 arc-second 2012 15 × 15 min IMG USGS NED ned19_n38x50_w106x25_co_arkansasvalley_2010 1/9 arc-second 2012 15 × 15 min IMG USGS NED ned19_n38x25_w106x50_co_sanluisvalley_2011 1/9 arc-second 2012 15 × 15 min IMG

State	Tiles of 10 m DEM
	USGS NED ned19_n39x50_w106x50_co_arkansasvalley_2010 1/9 arc-second 2012 15 × 15 min IMG
	USGS NED ned19_n38x75_w106x25_co_arkansasvalley_2010 1/9 arc-second 2012 15 × 15 min IMG
	USGS NED ned19_n39x00_w106x25_co_arkansasvalley_2010 1/9 arc-second 2012 15 × 15 min IMG
	USGS NED ned19_n38x25_w105x75_co_sanluisvalley_2011 1/9 arc-second 2012 15 × 15 min IMG
	USGS NED ned19_n39x75_w106x00_co_grandco_2010 1/9 arc-second 2011 15 × 15 min IMG
	USGS NED ned19_n38x00_w106x25_co_sanluisvalley_2011 1/9 arc-second 2012 15 × 15 min IMG
	USGS NED ned19_n38x00_w106x00_co_sanluisvalley_2011 1/9 arc-second 2012 15 × 15 min IMG
	USGS NED ned19_n38x00_w106x50_co_sanluisvalley_2011 1/9 arc-second 2012 15 × 15 min IMG
	USGS NED ned19_n38x00_w105x75_co_sanluisvalley_2011 1/9 arc-second 2012 15 × 15 min IMG
Nebraska	USGS NED ned19_n40x50_w100x25_ne_rainwater_2009 1/9 arc-second 2011 15 × 15 min IMG
	USGS NED ned19_n40x50_w100x00_ne_rainwater_2009 1/9 arc-second 2011 15 × 15 min IMG
	USGS NED ned19_n40x50_w100x50_ne_rainwater_2009 1/9 arc-second 2011 15 × 15 min IMG
	USGS NED ned19_n40x75_w100x75_ne_rainwater_2009 1/9 arc-second 2011 15 × 15 min IMG
	USGS NED ned19_n40x75_w100x00_ne_rainwater_2009 1/9 arc-second 2011 15 × 15 min IMG
	USGS NED ned19_n40x75_w100x25_ne_rainwater_2009 1/9 arc-second 2011 15 × 15 min IMG
	USGS NED ned19_n40x75_w100x50_ne_rainwater_2009 1/9 arc-second 2011 15 × 15 min IMG
	USGS NED ned19_n40x50_w100x75_ne_rainwater_2009 1/9 arc-second 2011 15 × 15 min IMG
	USGS NED ned19_n40x75_w101x00_ne_rainwater_2009 1/9 arc-second 2011 15 × 15 min IMG
	USGS NED ned19_n40x50_w101x00_ne_rainwater_2009 1/9 arc-second 2011 15 × 15 min IMG
	USGS NED ned19_n40x25_w100x00_ne_rainwater_2009 1/9 arc-second 2011 15 × 15 min IMG
	USGS NED ned19_n40x25_w100x50_ne_rainwater_2009 1/9 arc-second 2011 15 × 15 min IMG
	USGS NED ned19_n40x25_w100x25_ne_rainwater_2009 1/9 arc-second 2011 15 × 15 min IMG

State	Tiles of 10 m DEM
	USGS NED ned19_n40x25_w100x75_ne_rainwater_2009 1/9 arc-second 2011 15 × 15 min IMG
	USGS NED ned19_n41x00_w100x75_ne_rainwater_2009 1/9 arc-second 2011 15 × 15 min IMG
	USGS NED ned19_n41x00_w100x00_ne_rainwater_2009 1/9 arc-second 2011 15 × 15 min IMG
	USGS NED ned19_n41x00_w100x50_ne_rainwater_2009 1/9 arc-second 2011 15 × 15 min IMG
	USGS NED ned19_n41x00_w100x25_ne_rainwater_2009 1/9 arc-second 2011 15 × 15 min IMG
	USGS NED ned19_n40x75_w099x75_ne_rainwater_2009 1/9 arc-second 2011 15 × 15 min IMG
	USGS NED ned19_n40x50_w099x75_ne_rainwater_2009 1/9 arc-second 2011 15 × 15 min IMG
	USGS NED ned19_n40x25_w101x00_ne_rainwater_2009 1/9 arc-second 2011 15 × 15 min IMG
	USGS NED ned19_n41x00_w101x00_ne_rainwater_2009 1/9 arc-second 2011 15 × 15 min IMG
	USGS NED ned19_n40x25_w099x75_ne_rainwater_2009 1/9 arc-second 2011 15 × 15 min IMG
	USGS NED ned19_n41x00_w099x75_ne_rainwater_2009 1/9 arc-second 2011 15 × 15 min IMG
North Carolina	USGS NED ned19_n36x00_w081x50_nc_statewide_2003 1/9 arc-second 2012 15 × 15 min IMG
	USGS NED ned19_n36x00_w082x00_nc_statewide_2003 1/9 arc-second 2012 15 × 15 min IMG
	USGS NED ned19_n36x00_w081x25_nc_statewide_2003 1/9 arc-second 2012 15 × 15 min IMG
	USGS NED ned19_n36x00_w081x75_nc_statewide_2003 1/9 arc-second 2012 15 × 15 min IMG
	USGS NED ned19_n36x00_w081x00_nc_statewide_2003 1/9 arc-second 2012 15 × 15 min IMG
	USGS NED ned19_n36x00_w082x25_nc_statewide_2003 1/9 arc-second 2012 15 × 15 min IMG
	USGS NED ned19_n35x75_w082x00_nc_statewide_2003 1/9 arc-second 2012 15 × 15 min IMG
	USGS NED ned19_n35x75_w081x25_nc_statewide_2003 1/9 arc-second 2012 15 × 15 min IMG
	USGS NED ned19_n35x75_w081x50_nc_statewide_2003 1/9 arc-second 2012 15 × 15 min IMG
	USGS NED ned19_n35x75_w081x75_nc_statewide_2003 1/9 arc-second 2012 15 × 15 min IMG
	USGS NED ned19_n35x75_w081x00_nc_statewide_2003 1/9 arc-second 2012 15 × 15 min IMG

State	Tiles of 10 m DEM
	USGS NED ned19_n35x75_w082x25_nc_statewide_2003 1/9 arc-second 2012 15 × 15 min IMG
	USGS NED ned19_n36x25_w081x50_nc_statewide_2003 1/9 arc-second 2012 15 × 15 min IMG
	USGS NED ned19_n36x25_w081x00_nc_statewide_2003 1/9 arc-second 2012 15 × 15 min IMG
	USGS NED ned19_n36x25_w081x25_nc_statewide_2003 1/9 arc-second 2012 15 × 15 min IMG
	USGS NED ned19_n36x25_w082x00_nc_statewide_2003 1/9 arc-second 2012 15 × 15 min IMG
	USGS NED ned19_n36x25_w081x75_nc_statewide_2003 1/9 arc-second 2012 15 × 15 min IMG
	USGS NED ned19_n36x25_w082x25_nc_statewide_2003 1/9 arc-second 2012 15 × 15 min IMG
	USGS NED ned19_n36x00_w080x75_nc_statewide_2003 1/9 arc-second 2012 15 × 15 min IMG
	USGS NED ned19_n35x75_w080x75_nc_statewide_2003 1/9 arc-second 2012 15 × 15 min IMG
	USGS NED ned19_n36x25_w080x75_nc_statewide_2003 1/9 arc-second 2012 15 × 15 min IMG
Texas	USGS NED ned19_n31x50_w097x50_tx_bellburnetmclennancos_2011 1/9 arc-second 2012 15 × 15 min IMG
	USGS NED ned19_n31x25_w097x25_tx_bellburnetmclennancos_2011 1/9 arc-second 2012 15 × 15 min IMG
	USGS NED ned19_n31x00_w098x25_tx_bellburnetmclennancos_2011 1/9 arc-second 2012 15 × 15 min IMG
	USGS NED ned19_n31x25_w097x50_tx_bellburnetmclennancos_2011 1/9 arc-second 2012 15 × 15 min IMG
	USGS NED ned19_n31x50_w097x75_tx_bellburnetmclennancos_2011 1/9 arc-second 2012 15 × 15 min IMG
	USGS NED ned19_n31x75_w097x25_tx_bellburnetmclennancos_2011 1/9 arc-second 2012 15 × 15 min IMG
	USGS NED ned19_n31x25_w098x25_tx_bellburnetmclennancos_2011 1/9 arc-second 2012 15 × 15 min IMG
	USGS NED ned19_n31x00_w098x00_tx_bellburnetmclennancos_2011 1/9 arc-second 2012 15 ×× 15 min IMG
	USGS NED ned19_n31x25_w097x75_tx_bellburnetmclennancos_2011 1/9 arc-second 2012 15 × 15 min IMG
	USGS NED ned19_n31x00_w097x50_tx_bellburnetmclennancos_2011 1/9 arc-second 2012 15 × 15 min IMG
	USGS NED ned19_n31x00_w097x75_tx_bellburnetmclennancos_2011 1/9 arc-second 2012 15 × 15 min IMG
	USGS NED ned19_n31x75_w097x50_tx_bellburnetmclennancos_2011 1/9 arc-second 2012 15 × 15 min IMG

State	Tiles of 10 m DEM
	USGS NED ned19_n31x25_w098x00_tx_bellburnetmclennancos_2011 1/9 arc-second 2012 15 × 15 min IMG
	USGS NED ned19_n31x00_w097x25_tx_bellburnetmclennancos_2011 1/9 arc-second 2012 15 × 15 min IMG
	USGS NED ned19_n31x50_w097x25_tx_bellburnetmclennancos_2011 1/9 arc-second 2012 15 × 15 min IMG
	USGS NED ned19_n30x75_w098x25_tx_bellburnetmclennancos_2011 1/9 arc-second 2012 15 × 15 min IMG
	USGS NED ned19_n30x75_w098x00_tx_bellburnetmclennancos_2011 1/9 arc-second 2012 15 × 15 min IMG
	USGS NED ned19_n30x75_w097x50_tx_bellburnetmclennancos_2011 1/9 arc-second 2012 15 × 15 min IMG
	USGS NED ned19_n30x75_w098x00_tx_central_llano_2007 1/9 arc-second 2010 15 × 15 min IMG
	USGS NED ned19_n30x75_w098x25_tx_central_llano_2007 1/9 arc-second 2010 15 × 15 min IMG
	USGS NED ned19_n31x75_w097x00_tx_bellburnetmclennancos_2011 1/9 arc-second 2012 15 × 15 min IMG
	USGS NED ned19_n31x50_w097x00_tx_bellburnetmclennancos_2011 1/9 arc-second 2012 15 × 15 min IMG
	USGS NED ned19_n31x25_w098x50_tx_central_llano_2007 1/9 arc-second 2010 15 × 15 min IMG
	USGS NED ned19_n31x50_w098x50_tx_central_llano_2007 1/9 arc-second 2010 15 × 15 min IMG
	USGS NED ned19_n31x00_w098x50_tx_central_llano_2007 1/9 arc-second 2010 15 × 15 min IMG
	USGS NED ned19_n31x75_w098x50_tx_central_llano_2007 1/9 arc-second 2010 15 × 15 min IMG
	USGS NED ned19_n31x00_w098x50_tx_bellburnetmclennancos_2011 1/9 arc-second 2012 15 × 15 min IMG
	USGS NED ned19_n30x75_w098x50_tx_central_llano_2007 1/9 arc-second 2010 15 × 15 min IMG
	USGS NED ned19_n30x75_w098x50_tx_bellburnetmclennancos_2011 1/9 arc-second 2012 15 × 15 min IMG
Washington	USGS NED ned19_n48x50_w122x00_wa_northpugetsound_2006 1/9 arc-second 2009 15 × 15 min IMG
	USGS NED ned19_n48x50_w122x50_wa_puget_sound_2000 1/9 arc-second 2012 15 × 15 min IMG
	USGS NED ned19_n48x50_w121x50_wa_northpugetsound_2006 1/9 arc-second 2009 15 × 15 min IMG
	USGS NED ned19_n49x00_w122x50_wa_northpugetsound_2006 1/9 arc-second 2009 15 × 15 min IMG
	USGS NED ned19_n48x75_w122x75_wa_sanjuanco_2009 1/9 arc-second 2011 15 × 15 min IMG

State	Tiles of 10 m DEM
	USGS NED ned19_n48x50_w122x25_wa_northpugetsound_2006 1/9 arc-second 2009 15 × 15 min IMG
	USGS NED ned19_n48x75_w121x25_wa_northpugetsound_2006 1/9 arc-second 2009 15 × 15 min IMG
	USGS NED ned19_n49x00_w121x25_wa_northpugetsound_2006 1/9 arc-second 2009 15 × 15 min IMG
	USGS NED ned19_n49x00_w122x00_wa_northpugetsound_2006 1/9 arc-second 2009 15 × 15 min IMG
	USGS NED ned19_n48x50_w122x75_wa_puget_sound_2000 1/9 arc-second 2012 15 × 15 min IMG
	USGS NED ned19_n48x75_w122x00_wa_northpugetsound_2006 1/9 arc-second 2009 15 × 15 min IMG
	USGS NED ned19_n48x75_w122x75_wa_northpugetsound_2006 1/9 arc-second 2009 15 × 15 min IMG
	USGS NED ned19_n48x75_w121x75_wa_northpugetsound_2006 1/9 arc-second 2009 15 × 15 min IMG
	USGS NED ned19_n48x75_w122x25_wa_northpugetsound_2006 1/9 arc-second 2009 15 × 15 min IMG
	USGS NED ned19_n49x00_w121x75_wa_northpugetsound_2006 1/9 arc-second 2009 15 × 15 min IMG
	USGS NED ned19_n48x75_w122x50_wa_northpugetsound_2006 1/9 arc-second 2009 15 × 15 min IMG
	USGS NED ned19_n49x00_w122x25_wa_northpugetsound_2006 1/9 arc-second 2009 15 × 15 min IMG
	USGS NED ned19_n48x50_w122x50_wa_northpugetsound_2006 1/9 arc-second 2009 15 × 15 min IMG
	USGS NED ned19_n48x50_w122x75_wa_northpugetsound_2006 1/9 arc-second 2009 15 × 15 min IMG
	USGS NED ned19_n48x75_w121x50_wa_northpugetsound_2006 1/9 arc-second 2009 15 × 15 min IMG
	USGS NED ned19_n49x00_w122x75_wa_northpugetsound_2006 1/9 arc-second 2009 15 × 15 min IMG
	USGS NED ned19_n48x50_w121x75_wa_northpugetsound_2006 1/9 arc-second 2009 15 × 15 min IMG
	USGS NED ned19_n49x25_w122x25_wa_northpugetsound_2006 1/9 arc-second 2009 15 × 15 min IMG
	USGS NED ned19_n49x25_w122x50_wa_northpugetsound_2006 1/9 arc-second 2009 15 × 15 min IMG
	USGS NED ned19_n49x25_w122x00_wa_northpugetsound_2006 1/9 arc-second 2009 15 × 15 min IMG
	USGS NED ned19_n49x25_w122x75_wa_northpugetsound_2006 1/9 arc-second 2009 15 × 15 min IMG
	USGS NED ned19_n48x25_w122x50_wa_puget_sound_2000 1/9 arc-second 2012 15 × 15 min IMG

State	Tiles of 10 m DEM
	USGS NED ned19_n48x25_w122x75_wa_puget_sound_2000 1/9 arc-second 2012 15 × 15 min IMG
	USGS NED ned19_n48x50_w123x00_wa_puget_sound_2000 1/9 arc-second 2012 15 × 15 min IMG
	USGS NED ned19_n48x75_w123x00_wa_sanjuanco_2009 1/9 arc-second 2011 15 × 15 min IMG
	USGS NED ned19_n49x00_w123x00_wa_northpugetsound_2006 1/9 arc-second 2009 15 × 15 min IMG
	USGS NED ned19_n48x50_w123x00_wa_sanjuanco_2009 1/9 arc-second 2011 15 × 15 min IMG
	USGS NED ned19_n49x25_w123x00_wa_northpugetsound_2006 1/9 arc-second 2009 15 × 15 min IMG
	USGS NED ned19_n48x25_w123x00_wa_puget_sound_2000 1/9 arc-second 2012 15 × 15 min IMG
Louisiana	USGS NED ned19_n30x75_w091x50_la_statewide_2006 1/9 arc-second 2009 15 × 15 min IMG
	USGS NED ned19_n30x50_w091x00_la_statewide_2006 1/9 arc-second 2009 15 × 15 min IMG
	USGS NED ned19_n30x50_w091x50_la_atchafalayabasin_2010 1/9 arc-second 2011 15 × 15 min IMG
	USGS NED ned19_n30x50_w091x50_la_statewide_2006 1/9 arc-second 2009 15 × 15 min IMG
	USGS NED ned19_n30x75_w091x00_la_statewide_2006 1/9 arc-second 2009 15 × 15 min IMG
	USGS NED ned19_n30x75_w091x25_la_statewide_2006 1/9 arc-second 2009 15 × 15 min IMG
	USGS NED ned19_n30x75_w090x75_la_statewide_2006 1/9 arc-second 2009 15 × 15 min IMG
	USGS NED ned19_n30x50_w091x25_la_statewide_2006 1/9 arc-second 2009 15 × 15 min IMG
	USGS NED ned19_n30x50_w090x75_la_statewide_2006 1/9 arc-second 2009 15 × 15 min IMG
	USGS NED ned19_n30x50_w091x50_LA-USGS_Atchafalaya2_2012_2014 1/9 arc-second 20140615 15 15 min IMG
	USGS NED ned19_n31x00_w091x50_la_statewide_2006 1/9 arc-second 2009 15 × 15 min IMG
	USGS NED ned19_n31x00_w091x25_la_statewide_2006 1/9 arc-second 2009 15 × 15 min IMG
	USGS NED ned19_n31x00_w091x00_la_statewide_2006 1/9 arc-second 2009 15 × 15 min IMG
	USGS NED ned19_n31x00_w090x75_la_statewide_2006 1/9 arc-second 2009 15 × 15 min IMG
	USGS NED ned19_n30x25_w091x00_la_statewide_2006 1/9 arc-second 2009 15 × 15 min IMG

State	Tiles of 10 m DEM
	USGS NED ned19_n30x25_w091x50_la_atchafalayabasin_2010 1/9 arc-second 2011 15 × 15 min IMG
	USGS NED ned19_n30x25_w091x50_la_statewide_2006 1/9 arc-second 2009 15 × 15 min IMG
	USGS NED ned19_n30x25_w090x75_la_statewide_2006 1/9 arc-second 2009 15 × 15 min IMG
	USGS NED ned19_n30x25_w091x25_la_statewide_2006 1/9 arc-second 2009 15 × 15 min IMG
	USGS NED ned19_n30x25_w091x50_LA-USGS_Atchafalaya2_2012_2014 1/9 arc-second 20140615 15 × 15 min IMG
	USGS NED ned19_n30x25_w091x25_LA-USGS_Atchafalaya2_2012_2014 1/9 arc-second 20140615 15 × 15 min IMG
	USGS NED ned19_n30x75_w090x50_la_statewide_2006 1/9 arc-second 2009 15 × 15 min IMG
	USGS NED ned19_n30x50_w090x50_la_statewide_2006 1/9 arc-second 2009 15 × 15 min IMG
	USGS NED ned19_n30x75_w091x75_la_statewide_2006 1/9 arc-second 2009 15 × 15 min IMG
	USGS NED ned19_n30x50_w091x75_la_atchafalayabasin_2010 1/9 arc-second 2011 15 × 15 min IMG
	USGS NED ned19_n30x50_w091x75_la_statewide_2006 1/9 arc-second 2009 15 × 15 min IMG
	USGS NED ned19_n30x75_w091x75_la_atchafalayabasin_2010 1/9 arc-second 2011 15 × 15 min IMG
	USGS NED ned19_n30x75_w091x75_LA-USGS_Atchafalaya2_2012_2014 1/9 arc-second 20140615 15 × 15 min IMG
	USGS NED ned19_n30x50_w091x75_LA-USGS_Atchafalaya2_2012_2014 1/9 arc-second 20140615 15 × 15 min IMG
	USGS NED ned19_n31x00_w090x50_la_statewide_2006 1/9 arc-second 2009 15 × 15 min IMG
	USGS NED ned19_n30x25_w090x50_la_statewide_2006 1/9 arc-second 2009 15 × 15 min IMG
	USGS NED ned19_n31x00_w091x75_la_statewide_2006 1/9 arc-second 2009 15 × 15 min IMG
	USGS NED ned19_n31x00_w091x75_LA-USGS_Atchafalaya2_2012_2014 1/9 arc-second 20140615 15 × 15 min IMG
	USGS NED ned19_n30x25_w091x75_la_atchafalayabasin_2010 1/9 arc-second 2011 15 × 15 min IMG
	USGS NED ned19_n30x25_w091x75_la_statewide_2006 1/9 arc-second 2009 15 × 15 min IMG
	USGS NED ned19_n30x25_w091x75_LA-USGS_Atchafalaya2_2012_2014 1/9 arc-second 20140615 15 × 15 min IMG

Tiles of 30 m DEMs

The following tiles are available to download in USGS TNM Download: https://viewer.nationalmap.gov/basic/

State	Tiles of 30 m DEM
Colorado	USGS NED 1/3 arc-second n40w107
	USGS NED n39w107 1/3 arc-second
	USGS NED 1/3 arc-second n40w106
	USGS NED 1/3 arc-second n39w106
Nebraska	USGS NED 1/3 arc-second n41w101 1 x 1 degree ArcGrid 2019
	USGS NED 1/3 arc-second n41w100 1 x 1 degree ArcGrid 2019
North Carolina	USGS NED 1/3 arc-second n36w082 1 x 1 degree ArcGrid 2019
	USGS NED n36w081 1/3 arc-second 2013 1 x 1 degree ArcGrid
	USGS NED 1/3 arc-second n36w083 1 x 1 degree ArcGrid 2017
	USGS NED 1/3 arc-second n37w082 1 x 1 degree ArcGrid 2019
	USGS NED 1/3 arc-second n37w081 1 x 1 degree ArcGrid 2018
	USGS NED 1/3 arc-second n37w083 1 x 1 degree ArcGrid 2018
Texas	USGS NED 1/3 arc-second n32w098 1 x 1 degree ArcGrid 2019
	USGS NED 1/3 arc-second n31w098 1 x 1 degree ArcGrid 2019
	USGS NED 1/3 arc-second n32w099 1 x 1 degree ArcGrid 2019
	USGS NED 1/3 arc-second n31w099 1 x 1 degree ArcGrid 2019
	USGS NED 1/3 arc-second n32w097 1 x 1 degree ArcGrid 2019
	USGS NED 1/3 arc-second n31w097 1 x 1 degree ArcGrid 2019
Washington	USGS NED 1/3 arc-second n49w122 1 x 1 degree ArcGrid 2018
	USGS NED 1/3 arc-second n49w123 1 x 1 degree ArcGrid 2019
	USGS NED 1/3 arc-second n50w122 1 x 1 degree ArcGrid 2018
	USGS NED 1/3 arc-second n49w121 1 x 1 degree ArcGrid 2018
	USGS NED 1/3 arc-second n50w123 1 x 1 degree ArcGrid 2018
Louisiana	USGS NED 1/3 arc-second n31w091 1 x 1 degree ArcGrid 2019
	USGS NED 1/3 arc-second n31w092 1 x 1 degree ArcGrid 2019

Tiles of 100 m and 1000 m DEMs

The following tiles are available to download in USGS's website: https://dds.cr.usgs.gov/srtm/version2_1/

States	Tiles 100 m DEM	Tiles 1000 m DEM
Colorado	N38W107.SRTMGL3	w140n40.SRTM30
	N39W107.SRTMGL3	
	N39W106.SRTMGL3	
	N38W106.SRTMGL3	
Nebraska	N40W100.SRTMGL3	w140n90.SRTM30
	N40W101.SRTMGL3	
North Carolina	N35W082.SRTMGL3	w140n90.SRTM30
	N35W081.SRTMGL3	
	N35W083.SRTMGL3	
Texas	N29W098.SRTMGL3	
	N29W099.SRTMGL3	
Washington	N48W123.SRTMGL3	w100n40.SRTM30
	N48W122.SRTMGL3	
Louisiana	N29W091.SRTMGL3	w100n40.SRTM30
	N29W092.SRTMGL3	

Tables of the analysis results

Table A1. Residual, Average Residual, RMSE and Processing Time for Washington. Interpolation Methods Include (in Top-to-Bottom Order) Bicubic, Bilinear, and Biquadratic polynomials, Closest Centroid, Nearest Neighbor, Triangulated Irregular Network, and Weighted Average

Resolution	Study area	Interpolation method	Avg. residual (m)	Avg. time (s)	Avg. ratio of residual	RMSE (m)
10	Washington	biCub	−474.29	23.160	−0.01608	598.25
10	Washington	biLin	−275.87	21.059	−0.00942	354.63
10	Washington	biQua	−350.39	21.651	−0.01191	444.94
10	Washington	clos	1,317.03	19.142	0.04514	1,665.34
10	Washington	NN	−878.59	22.620	−0.02975	1,108.14
10	Washington	TIN	−776.38	41.305	−0.02623	975.04
10	Washington	wavg	37.99	19.690	0.00135	99.64
30	Washington	biCub	−319.35	2.004	−0.01089	399.54
30	Washington	biLin	−136.67	1.173	−0.00471	173.10
30	Washington	biQua	−210.48	1.430	−0.00717	262.71
30	Washington	clos	1,069.14	0.817	0.03723	1,371.21
30	Washington	NN	−567.18	5.546	−0.01943	722.40
30	Washington	TIN	−476.51	11.348	−0.01611	598.79
30	Washington	wavg	74.51	0.865	0.00269	130.65
100	Washington	biCub	−306.76	0.503	−0.01050	402.13
100	Washington	biLin	−175.48	0.273	−0.00599	237.11
100	Washington	biQua	−217.31	0.340	−0.00728	290.31
100	Washington	clos	698.93	0.204	0.02469	915.64
100	Washington	NN	−411.20	1.650	−0.01399	532.32
100	Washington	TIN	−318.37	3.383	−0.01065	416.41
100	Washington	wavg	−22.26	0.201	−0.00032	111.77
1,000	Washington	biCub	−239.50	0.108	−0.00719	548.59
1,000	Washington	biLin	−200.71	0.077	−0.00754	516.00
1,000	Washington	biQua	−222.57	0.083	−0.00850	543.43
1,000	Washington	clos	299.99	0.068	0.01204	578.81
1,000	Washington	NN	−223.18	0.147	−0.00760	529.18
1,000	Washington	TIN	−161.48	0.450	−0.00758	471.21
1,000	Washington	wavg	−129.89	0.068	−0.00484	496.20

Table A2. Residual, Average Residual, RMSE and Processing Time for North Carolina. Interpolation Methods Include (in Top-to-Bottom Order) Bicubic, Bilinear, and Biquadratic polynomials, Closest Centroid, Nearest Neighbor, Triangulated Irregular Network, and Weighted Average

Resolution	Study Area	Method	Avg. residual	Avg. time	Avg. ratio of residual	RMSE
10	North Carolina	biCub	−392.80	82.186	−0.00973	497.17
10	North Carolina	biLin	−255.92	78.635	−0.00643	326.27
10	North Carolina	biQua	−305.51	79.250	−0.00761	387.26
10	North Carolina	clos	1,031.91	75.460	0.02535	1,317.31
10	North Carolina	NN	−795.94	34.227	−0.01958	1,015.06
10	North Carolina	TIN	−754.26	72.281	−0.01853	951.92
10	North Carolina	wavg	−8.86	76.333	−0.00033	71.50
30	North Carolina	biCub	−362.34	4.078	−0.00897	467.52
30	North Carolina	biLin	−180.32	2.678	−0.00452	231.91
30	North Carolina	biQua	−252.72	3.131	−0.00626	325.12
30	North Carolina	clos	794.56	1.949	0.01972	1,013.90
30	North Carolina	NN	−547.25	10.186	−0.01360	717.20
30	North Carolina	TIN	−523.88	20.687	−0.01293	666.72
30	North Carolina	wavg	−37.93	2.088	−0.00093	64.29
100	North Carolina	biCub	−382.45	0.921	−0.00938	505.19
100	North Carolina	biLin	−308.36	0.499	−0.00754	407.88
100	North Carolina	biQua	−339.05	0.624	−0.00835	447.64
100	North Carolina	clos	99.81	0.357	0.00278	195.06
100	North Carolina	NN	−419.75	2.560	−0.01046	559.73
100	North Carolina	TIN	−398.08	5.935	−0.00986	520.72
100	North Carolina	wavg	−252.05	0.364	−0.00618	330.92
1,000	North Carolina	biCub	−139.16	0.122	−0.00105	641.36
1,000	North Carolina	biLin	−109.73	0.091	−0.00167	623.53
1,000	North Carolina	biQua	−140.67	0.096	−0.00124	643.46
1,000	North Carolina	clos	−50.74	0.083	−0.00054	610.34
1,000	North Carolina	NN	−146.28	0.120	−0.00200	639.84
1,000	North Carolina	TIN	−122.87	0.468	−0.00255	623.09
1,000	North Carolina	wavg	−131.94	0.081	−0.00080	630.61

Table A3. Residual, Average Residual, RMSE and Processing Time for Colorado. Interpolation Methods Include (in Top-to-Bottom Order) Bicubic, Bilinear, and Biquadratic Polynomials, Closest Centroid, Nearest Neighbor, Triangulated Irregular Network, and Weighted Average

Resolution	Study Area	Method	Avg. residual	Avg. time	Avg. ratio of residual	RMSE
10	Colorado	biCub	−210.68	7.957	−0.00968	287.08
10	Colorado	biLin	−119.97	5.588	−0.00566	168.04
10	Colorado	biQua	−155.91	6.381	−0.00729	215.30
10	Colorado	clos	604.24	4.200	0.02749	780.32
10	Colorado	NN	−356.98	17.031	−0.01629	506.09
10	Colorado	TIN	−426.32	29.384	−0.01930	566.54
10	Colorado	wavg	14.10	4.499	0.00046	58.55
30	Colorado	biCub	−180.84	1.800	−0.00808	246.28
30	Colorado	biLin	−84.22	1.095	−0.00382	119.82
30	Colorado	biQua	−124.50	1.309	−0.00560	172.11
30	Colorado	clos	451.83	0.729	0.02082	588.73
30	Colorado	NN	−264.50	3.091	−0.01182	372.96
30	Colorado	TIN	−292.40	7.784	−0.01326	392.15
30	Colorado	wavg	−5.13	0.798	−0.00020	55.06
100	Colorado	biCub	−188.86	0.520	−0.00839	258.17
100	Colorado	biLin	−134.41	0.311	−0.00593	189.08
100	Colorado	biQua	−155.35	0.367	−0.00703	214.44
100	Colorado	clos	164.14	0.208	0.00757	242.11
100	Colorado	NN	−199.98	0.736	−0.00922	282.23
100	Colorado	TIN	−211.86	2.349	−0.00992	286.12
100	Colorado	wavg	−93.35	0.226	−0.00413	143.08
1,000	Colorado	biCub	−96.85	0.077	−0.00350	630.70
1,000	Colorado	biLin	−62.77	0.059	0.00636	633.64
1,000	Colorado	biQua	−64.57	0.061	0.00222	586.04
1,000	Colorado	clos	−9.11	0.054	0.00077	597.91
1,000	Colorado	NN	−91.66	0.078	0.00324	599.84
1,000	Colorado	TIN	−86.85	0.234	−0.00152	590.84
1,000	Colorado	wavg	−38.11	0.054	0.00378	577.50

Table A4. Residual, Average Residual, RMSE and Processing Time for Nebraska. Interpolation Methods Include (in Top-to-Bottom Order) Bicubic, Bilinear, and Biquadratic polynomials, Closest Centroid, Nearest Neighbor, Triangulated Irregular Network, and Weighted Average

Resolution	Study Area	Method	Avg. residual	Avg. time	Avg. ratio of residual	RMSE
10	Nebraska	biCub	−155.07	15.751	−0.00438	184.23
10	Nebraska	biLin	−87.86	12.139	−0.00249	105.16
10	Nebraska	biQua	−116.45	13.238	−0.00329	138.50
10	Nebraska	clos	363.39	9.779	0.01024	428.17
10	Nebraska	NN	−246.60	15.574	−0.00693	291.90
10	Nebraska	TIN	−241.93	35.472	−0.00681	285.92
10	Nebraska	wavg	−18.45	10.406	−0.00054	28.50
30	Nebraska	biCub	−122.90	2.861	−0.00345	148.07
30	Nebraska	biLin	−66.32	1.831	−0.00187	81.23
30	Nebraska	biQua	−95.44	2.162	−0.00269	115.07
30	Nebraska	clos	239.39	1.287	0.00676	283.16
30	Nebraska	NN	−158.98	4.681	−0.00447	189.61
30	Nebraska	TIN	−153.91	10.863	−0.00436	183.12
30	Nebraska	wavg	−38.88	1.374	−0.00111	50.14
100	Nebraska	biCub	−93.37	0.776	−0.00268	120.40
100	Nebraska	biLin	−77.33	0.470	−0.00222	104.34
100	Nebraska	biQua	−83.26	0.560	−0.00232	111.35
100	Nebraska	clos	16.40	0.330	0.00043	58.37
100	Nebraska	NN	−101.37	1.126	−0.00282	130.97
100	Nebraska	TIN	−97.17	3.289	−0.00271	126.20
100	Nebraska	wavg	−68.60	0.341	−0.00198	97.01
1,000	Nebraska	biCub	−5.99	0.131	0.00065	443.39
1,000	Nebraska	biLin	−8.46	0.090	0.00058	457.28
1,000	Nebraska	biQua	−7.15	0.098	0.00009	426.08
1,000	Nebraska	clos	0.70	0.076	−0.00046	439.67
1,000	Nebraska	NN	−21.65	0.120	−0.00030	448.87
1,000	Nebraska	TIN	0.49	0.437	0.00077	452.23
1,000	Nebraska	wavg	−6.58	0.077	−0.00055	443.66

Table A5. Residual, Average Residual, RMSE and Processing Time for Texas. Interpolation Methods Include (in Top-to-Bottom Order) Bicubic, Bilinear, and Biquadratic Polynomials, Closest Centroid, Nearest Neighbor, Triangulated Irregular Network, and Weighted Average

Resolution	Study Area	Method	Avg. residual	Avg. time	Avg. ratio of residual	RMSE
10	Texas	biCub	−66.78	13.527	−0.00195	81.42
10	Texas	biLin	−46.30	10.210	−0.00135	56.78
10	Texas	biQua	−56.03	11.303	−0.00164	68.29
10	Texas	clos	109.90	8.228	0.00317	140.87
10	Texas	NN	−92.74	16.384	−0.00269	115.54
10	Texas	TIN	−96.19	34.548	−0.00280	118.34
10	Texas	wavg	−22.83	8.734	−0.00067	29.10
30	Texas	biCub	−42.88	2.730	−0.00129	55.29
30	Texas	biLin	−26.93	1.761	−0.00087	36.43
30	Texas	biQua	−33.88	2.076	−0.00098	44.47
30	Texas	clos	76.99	1.241	0.00218	103.94
30	Texas	NN	−57.02	3.433	−0.00171	73.55
30	Texas	TIN	−55.18	9.743	−0.00169	70.44
30	Texas	wavg	−14.67	1.330	−0.00047	25.10
100	Texas	biCub	−31.55	0.775	−0.00107	64.98
100	Texas	biLin	−24.25	0.481	−0.00080	61.96
100	Texas	biQua	−29.45	0.565	−0.00079	64.93
100	Texas	clos	40.61	0.338	0.00099	74.31
100	Texas	NN	−36.77	0.815	−0.00113	70.56
100	Texas	TIN	−36.22	3.066	−0.00121	70.66
100	Texas	wavg	−19.31	0.355	−0.00081	59.64
1,000	Texas	biCub	9.29	0.106	0.00991	601.13
1,000	Texas	biLin	1.95	0.078	0.01138	613.45
1,000	Texas	biQua	8.70	0.082	0.01353	622.86
1,000	Texas	clos	2.20	0.069	0.00922	616.65
1,000	Texas	NN	25.42	0.097	0.00987	610.91
1,000	Texas	TIN	−15.79	0.339	0.00748	633.42
1,000	Texas	wavg	−2.18	0.069	0.00829	610.30

Table A6. Residual, Average Residual, RMSE and Processing Time for Louisiana. Interpolation Methods Include (in top-to-bottom order) Bicubic, Bilinear, and Biquadratic polynomials, Closest Centroid, Nearest Neighbor, Triangulated Irregular Network, and Weighted Average

Resolution	Study Area	Method	Avg. residual	Avg. time	Avg. ratio of residual	RMSE
10	Louisiana	biCub	−31.32	25.881	−0.00084	38.44
10	Louisiana	biLin	−22.62	22.476	−0.00061	27.93
10	Louisiana	biQua	−27.22	23.573	−0.00073	33.43
10	Louisiana	clos	25.51	19.252	0.00070	31.80
10	Louisiana	NN	−32.94	27.879	−0.00088	40.26
10	Louisiana	TIN	−33.80	51.336	−0.00091	41.15
10	Louisiana	wavg	−18.00	20.357	−0.00048	22.23
30	Louisiana	biCub	−16.36	2.924	−0.00048	25.76
30	Louisiana	biLin	−12.84	1.806	−0.00036	22.00
30	Louisiana	biQua	−15.01	2.171	−0.00042	24.82
30	Louisiana	clos	4.86	1.288	0.00013	17.56
30	Louisiana	NN	−16.45	7.183	−0.00045	25.88
30	Louisiana	TIN	−16.42	14.367	−0.00046	25.63
30	Louisiana	wavg	−11.54	1.367	−0.00030	21.29
100	Louisiana	biCub	−7.06	0.792	−0.00014	53.29
100	Louisiana	biLin	−8.18	0.492	−0.00019	54.58
100	Louisiana	biQua	−5.32	0.579	−0.00017	53.48
100	Louisiana	clos	−5.43	0.330	−0.00003	53.61
100	Louisiana	NN	−7.89	0.772	−0.00020	53.75
100	Louisiana	TIN	−9.16	3.179	−0.00025	56.44
100	Louisiana	wavg	−6.40	0.361	−0.00009	55.85
1,000	Louisiana	biCub	4.94	0.109	0.00265	584.24
1,000	Louisiana	biLin	17.30	0.079	0.00215	593.02
1,000	Louisiana	biQua	8.39	0.084	0.00325	613.95
1,000	Louisiana	clos	7.44	0.067	0.00203	603.86
1,000	Louisiana	NN	−1.19	0.112	0.00123	602.79
1,000	Louisiana	TIN	14.16	0.369	0.00168	599.01
1,000	Louisiana	wavg	12.11	0.070	0.00236	595.14

References

Bolstad, P. (2019). GIS Fundamentals: A First Text on Geographic Information systems, 6th ed., Ann Arbor, MI: XanEdu Publishing Inc.

Buttenfield, B., M. Ghandehari, S. Leyk, L. Stanislawski, M. Brantley, Y. Qiang. (2016). Measuring Distance "As the Horse Runs": Cross-Scale Comparison of Terrain-Based Metrics. *International Conference on GIScience Short Paper Proceedings* 1. http://dx.doi.org/10.21433/b3118rh987cz

Chang, K., and B. Tsai. (1991). "The Effect of DEM Resolution on Slope and Aspect Mapping." *Cartography and Geographic Information Systems* 18(1), 69–77. https://doi.org/10.1559/152304091783805626.

GDAL/OGR contributors. (2020). GDAL/OGR GEOSPATIAL Data Abstraction Software Library. Open Source Geospatial Foundation. https://gdal.org

Gesch, D. B. (2007). "The National Elevation Dataset." In Digital Elevation Model Technologies and Applications: The DEM Users Manual, 2nd ed., 99–118.

Gesch, D.B., M. J. Oimoen, and G. A. Evans. (2014). "Accuracy Assessment of the U.S. Geological Survey National Elevation Dataset, and Comparison with Other Large-Area Elevation Datasets: SRTM and ASTER." Report No. 2014–1008; Open-File Report, p. 18, USGS Publications Warehouse. https://doi.org/10.3133/ofr20141008.

Ghandehari, M. (2019). Cross-Scale Analysis of Surface-Adjusted Measurements in digital Elevation Models, Doctoral dissertation. University of Colorado, Boulder.

Ghandehari, M., and B. Buttenfield. (2018). "Slope-Adjusted Surface Area Computations in Digital Terrain." Proceedings of 5th International Conference of the International Society of Geomorphometry (Geomorphometry 2018).

Ghandehari, M., B. P. Buttenfield, C. J. Q. Farmer. (2019). Comparing the accuracy of estimated terrain elevations across spatial resolution. *International Journal of Remote Sensing* 40(13), 5025–5049. http://dx.doi.org/10.1080/01431161.2019.1577581

Gutiérrez, M. (2012). "Chapter 15.3 Applied Geomorphology in Periglacial Regins." In Geomorphology, 601–13. Boca Raton, FL: Taylor & Francis.

Harms, T. K., E. A. Wentz, and N. B. Grimm. (2009). "Spatial Heterogeneity of Denitrification in Semi-Arid Floodplains." *Ecosystems* 12(1), 129–43. https://doi.org/10.1007/s10021-008-9212-6.

Hutchinson, M. F., and J. C. Gallant. (2000). Digital Elevation Models and Representation of Terrain Shape. https://publications.csiro.au/rpr/pub?list=BRO&pid=procite:46f1de5d-172e-4f8e-8696-da3b6f7b03ca.

Jenness, J. S. (2004). "Calculating Landscape Surface Area from Digital Elevation Models." *Wildlife Society Bulletin* 32(3), 829–39. https://doi.org/10.2193/0091-7648(2004)032[0829:CLSAFD]2.0.CO;2.

Kienzle, S. (2004). "The Effect of DEM Raster Resolution on First Order, Second Order and Compound Terrain Derivatives." *Transactions in GIS* 8(1), 83–111. https://doi.org/10.1111/j.1467-9671.2004.00169.x.

Kiessling, F., P. Nefzger, J. Nolasco, and U. Kaintzyk. (2014). Overhead Power Lines: Planning, Design, Construction. Berlin, Germany: Springer.

Montello, D. R. (2001). "Scale in Geography." In International Encyclopedia of the Social and Behavioral Sciences, 13501–4, edited by N. J. Smelser and B. Baltes.

Oliphant, T. E. (2006). A guide to NumPy (Vol. 1), Trelgol Publishing USA.

Qiang, Y., B. P. Buttenfield, N. Lam, and N. V. de Weghe. (2018). "Novel Models for Multi-Scale Spatial and Temporal Analyses." In 10th International Conference on Geographic Information Science (GIScience 2018), Vol. 114, 55:1–55:7. edited by S. Winter, A. Griffin, & M. Sester. Dagstuhl, Germany: Schloss Dagstuhl–Leibniz-Zentrum fuer Informatik. https://doi.org/10.4230/LIPIcs.GISCIENCE.2018.55

Qiang, Y., and N. Van de Weghe. (2019). "Re-Arranging Space, Time and Scales in GIS: Alternative Models for Multi-Scale Spatio-Temporal Modeling and Analyses." *ISPRS International Journal of Geo-Information* 8(2), 72. https://doi.org/10.3390/ijgi8020072.

Quattrochi, D. A., and M. F. Goodchild. (1997). Scale in Remote Sensing and GIS. Boca Raton, FL: CRC Press.

Schneider, B. (2001). On the Uncertainty of Local Shape of Lines and Surfaces. *Cartography and Geographic Information Science* 28(4), 237–247. https://doi.org/10.1559/152304001782152991

Shafique, M., M. van der Meijde, N. Kerle, and F. van der Meer. (2011). "Impact of DEM Source and Resolution on Topographic Seismic Amplification." *International Journal of Applied Earth Observation and Geoinformation* 13(3), 420–7. https://doi.org/10.1016/j.jag.2010.09.005.

Shi, W. Z., and Y. Tian. (2006). "A Hybrid Interpolation Method for the Refinement of a Regular Grid Digital Elevation Model." *International Journal of Geographical Information Science* 20(1), 53–67. https://doi.org/10.1080/13658810500286943.

Sibson, R. (1981). "A Brief Description of Natural Neighbor Interpolation." In Interpolating Multivariate Data, 21–36. New York: John Wiley & Sons.

Stanislawski, L. V., J. Falgout, and B. P. Buttenfield. (2015). "Automated Extraction of Natural Drainage Density Patterns for the Conterminous United States through High-Performance Computing." *The Cartographic Journal* 52(2), 185–92. https://doi.org/10.1080/00087041.2015.1119466

Stoker, J. M. (2018). The US Geological Survey Physical Scientist. The Chief Elevation Scientist for the National Geospatial Program, personal communication (jstoker@usgs.gov) [Personal communication].

The IPython Development Team. (2018). Using IPython for parallel computing. https://ipyparallel.readthedocs.io/en/latest/.

Tucker, G. E., and G. R. Hancock. (2010). "Modelling Landscape Evolution." *Earth Surface Processes and Landforms* 35(1), 28–50. https://doi.org/10.1002/esp.1952.

University Corporation for Atmospheric Research (UCAR). (2004). Natgrid Introduction. http://www.ncarg.ucar.edu//ngmath/natgrid/nnhome.html.

Usery, E. L., M. P. Finn, D. J. Scheidt, S. Ruhl, T. Beard, and M. Bearden. (2004). "Geospatial Data Resampling and Resolution Effects on Watershed Modeling: A Case Study Using the Agricultural Non-Point Source Pollution Model." *Journal of Geographical Systems* 6(3), 289–306. https://doi.org/10.1007/s10109-004-0138-z.

Wilson, J. P. (2012). "Digital Terrain Modeling." *Geomorphology* 137(1), 107–21. https://doi.org/10.1016/j.geomorph.2011.03.012

Zhang, W., and D. R. Montgomery. (1994). "Digital Elevation Model Grid Size, Landscape Representation, and Hydrologic Simulations." *Water Resources Research* 30(4), 1019–28. https://doi.org/10.1029/93WR03553.